Application of Complex Geometrical Optics with Real Frequency (CGORF) for Modelling Scattering of Electromagnetic High-Frequency Waves on the Ionospheric Inhomogeneities

Yuriy Rapoport (1), Volodymyr Grimalsky (2), Andrzej Krankowski (1), Leszek Błaszkiewicz (1), Kacper Kotulak (1), Pawel Flisek (1), Sergei Petrishchevskii (3)

(1)University of Warmia and Mazury in Olsztyn, Poland;

(2) CIICAp, Autonomous University of State Morelos (UAEM), Cuernavaca, Mor., Mexico;

(3) Taras Shevchenko National University of Kyiv, Kyiv, Ukraine

LOFAR Family Meeting Olsztyn, Poland 12-16 June 2023

INTRODUCTION AND FORMULATION OF THE PROBLEM

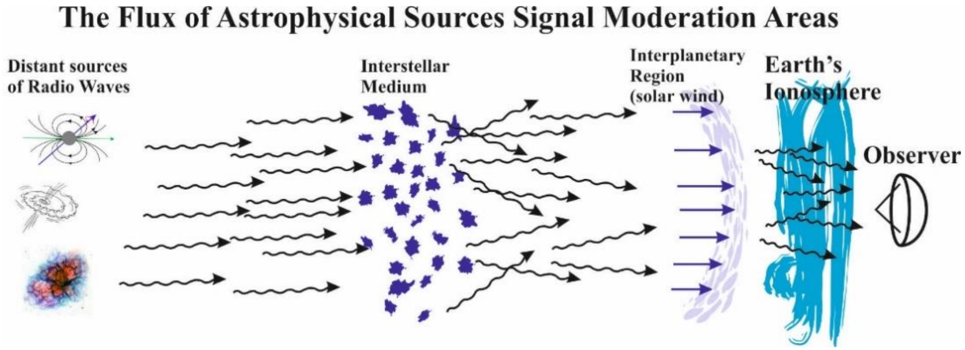

Typical locations in extra-terrestrial space where radio waves from astrophysical radiation sources (AGNs, SNRs and pulsars) are altered by an ionized medium. Both the interstellar and interplanetary mediums are extremely rarefied, although the radiation path is long in these regions. The ionosphere, on the other hand, is a much denser medium by comparison. Figure base on similar one from [Błaszkiewicz et al., 2020]

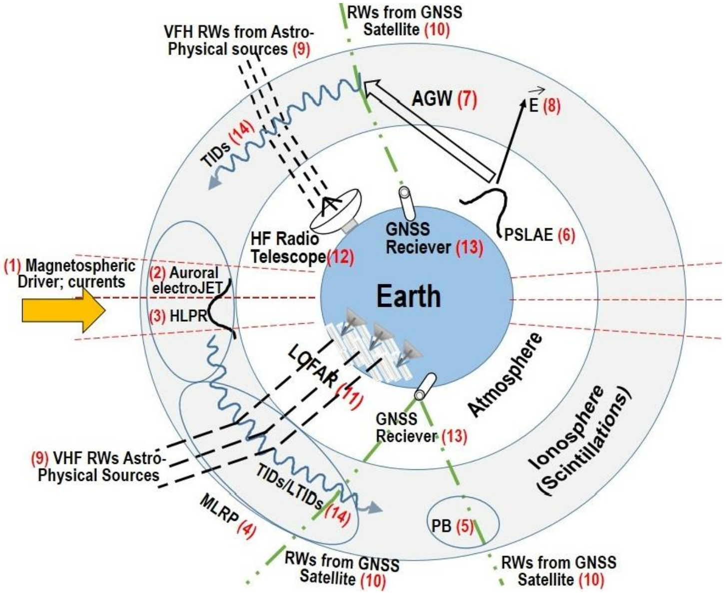

Simplified diagram of wave processes leading to ionospheric disturbances under investigation

Transition: Dynamic → Quasistatics with accounting for "previously lost quasi-magnetostatic" (magnetic) field. – I. Equations and boundary condition

$$\vec{\nabla}\times\vec{H} = ik_0\hat{\varepsilon}(\omega,\vec{r})\cdot\vec{E} + \frac{4\pi}{c}\vec{j}^{ext} \equiv \frac{4\pi}{c}\vec{j}; \qquad \hat{\varepsilon}(\omega,\vec{r}) = 1 - \frac{4\pi i\hat{\sigma}(\omega,\vec{r})}{\omega};$$

$$\vec{E} \approx -\vec{\nabla}\varphi, \quad or \quad \vec{\nabla}\times\vec{E} \approx 0 \qquad \vec{E},\vec{H} \sim e^{i(\omega t - k_x x - k_y y)}; \; k_0 \equiv \frac{\omega}{c};$$

(1) $$\vec{\nabla}\cdot(\hat{\varepsilon}(\omega,\vec{r})\cdot\vec{\nabla}\varphi) \approx 4\pi\rho^{ext}; \quad \rho^{ext} \equiv \frac{i}{\omega}\vec{\nabla}\cdot\vec{j}^{ext}.$$

$$\vec{j} = \vec{j}^{ext} + \frac{i\omega\hat{\varepsilon}(\omega,\vec{r})}{4\pi}\cdot\vec{E}; \quad \vec{\nabla}\cdot\vec{j} = 0;$$

$$\Delta\vec{H} = -\frac{4\pi}{c}\vec{\nabla}\times\vec{j}$$

(2) $$\frac{\partial^2 H_z}{\partial z^2} + \Delta H_z = \frac{\partial^2 H_z}{\partial z^2} - (k_x{}^2 + k_y{}^2)H_z = -\frac{4\pi}{c}(\vec{\nabla}\times\vec{j})_z = -\frac{4\pi}{c}\left(\frac{\partial j_y}{\partial x} - \frac{\partial j_x}{\partial y}\right)$$

Boundary condition at $z = z_{UP\,A}$

$$E_x = -Z_{21}H_x - Z_{22}H_y; \qquad E_y = Z_{11}H_x + Z_{12}H_y.$$

$$H_x = -\frac{i}{k_\perp{}^2}\left(\frac{4\pi}{c}k_y\sigma E_z + k_x\frac{dH_z}{dz}\right); \quad H_y = \frac{i}{k_\perp{}^2}\left(\frac{4\pi}{c}k_x\sigma E_z - k_y\frac{dH_z}{dz}\right); \quad E_z = -\frac{d\varphi}{dz};$$

(3) $$k_x\varphi = \frac{1}{k_\perp{}^2}\frac{4\pi}{c}\sigma(-k_y Z_{21} + k_x Z_{22})\frac{d\varphi}{dz} + \frac{1}{k_\perp{}^2}(k_x Z_{21} + k_y Z_{22})\frac{dH_z}{dz};$$

(4) $$k_y\varphi = \frac{1}{k_\perp{}^2}\frac{4\pi}{c}\sigma(k_y Z_{11} - k_x Z_{12})\frac{d\varphi}{dz} - \frac{1}{k_\perp{}^2}(k_x Z_{11} + k_y Z_{12})\frac{dH_z}{dz}; \qquad k_\perp{}^2 \equiv k_x{}^2 + k_y{}^2;$$

(5) Boundary condition at $z = 0;\ \varphi = 0;\ H_z = 0$

Equation (1), (2) with boundary conditions (3), (4) at $z = z_{UP\,A}$ and (5) at $z = 0$ determine entirely the solution of "dynamic-quasistatic" problem

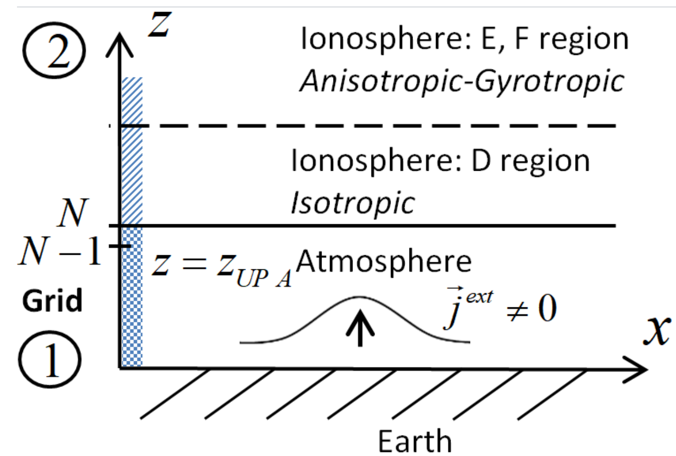

Grid points *N-1, N* to both region 1 and 2

Limiting pass: Transition → Quasistatics with accounting for “previously last quasi-magnetostatic” (magnetic) field – II. Effective tensor impedance on the atmosphere-ionosphere boundary: analytical-numerical combined model

From numerical scheme in the region 2; grid points *N, N-1* belongs to both regions 1 and 2

$$E_{x\ N} = b_{11}E_{x\ N-1} + b_{12}E_{x\ N-1};\ \ E_{y\ N} = b_{21}E_{x\ N-1} + b_{22}E_{x\ N-1};\ \ E_{x,y\ N} = E_{x,y\ N-1} + h_z\frac{\partial E_{x,y}}{\partial z}$$

at the surface between region 1 and 2 ($z \approx z_{UP\ A}$)

$$\frac{\partial E_x}{\partial z} \approx \frac{b_{11}-1}{h_z}E_x + \frac{b_{12}}{h_z}E_y;\ \ \frac{\partial E_y}{\partial z} \approx \frac{b_{21}}{h_z}E_x + \frac{b_{22}-1}{h_z}E_y$$

For isotropic case: $\Delta \equiv \varepsilon - \dfrac{k_x^2 + k_y^2}{k_0^2};\ \ \varepsilon = \varepsilon(\omega, z);\ \ k_0 = \dfrac{\omega}{c};$

$$H_x = -\frac{i}{\Delta k_0}\{k_x k_y \frac{\partial E_x}{\partial z} + (\varepsilon - \frac{k_x^2}{k_0^2})\frac{\partial E_y}{\partial z}\}$$

$$H_y = \frac{i}{\Delta k_0}\{(\varepsilon - \frac{k_y^2}{k_0^2})\frac{\partial E_x}{\partial z} + k_x k_y \frac{\partial E_y}{\partial z}\}$$

→ In grid form:

$$H_x = C_{11}E_x + C_{12}E_y$$

$$H_y = C_{21}E_x + C_{22}E_y$$

→

$$E_x = Z_{21}H_x + Z_{22}H_y;\ \ -E_y = Z_{11}H_x + Z_{12}H_y;\ \ D = C_{11}C_{22} - C_{12}C_{21}$$

$$Z_{21} = C_{22}/D;\ \ Z_{22} = -C_{12}/D;\ \ Z_{11} = -C_{11}/D;\ \ Z_{12} = C_{21}/D;$$

Complex anisotropic impedance is determined!

Numerical modelling (night) of penetration of ULF field with given current source: using new integrated dynamic-quasistatic model with inclusion quasimagnetostatic field, lost previously

$$\vec{j}_z^{\,ext} = J_m \exp\left[-\left(\frac{y-0.5L_x}{y_0}\right)^2 - \left(\frac{y-0.5L_x}{y_0{}^2}\right)^2 - \left(\frac{z-z_1}{z_0}\right)^2\right];\ [\vec{E}] = mV/m;\ [\vec{H}] = Oe \to 10^5\ nT;$$

$$J_m = 10^{-7}\ A/m^2;\ \theta = 10^\circ;\ x_0 = y_0 = 200\ km;\ z_1 = 20\ km;\ z_0 = 7\ km;\ L_x = L_y = 5000\ km;\ \boldsymbol{\omega = 2\pi f = 0.01\ s^{-1}}$$

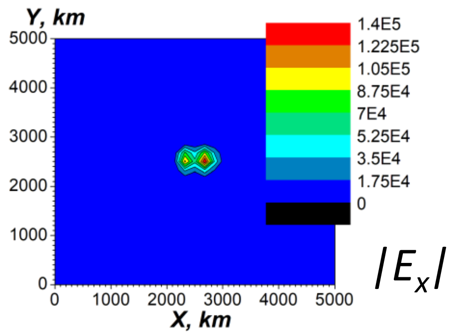

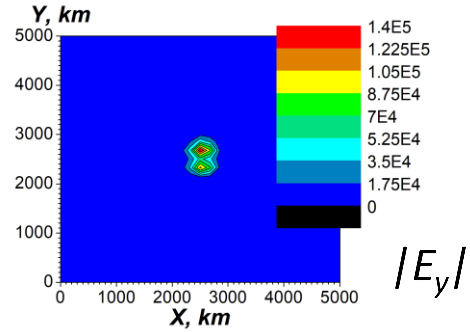

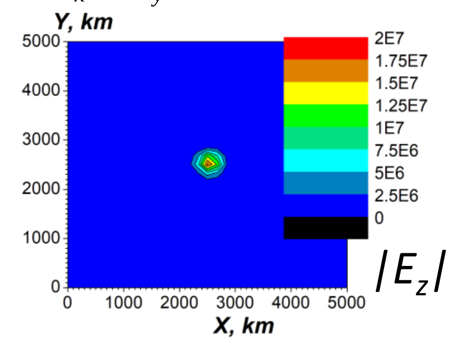

z=60 km

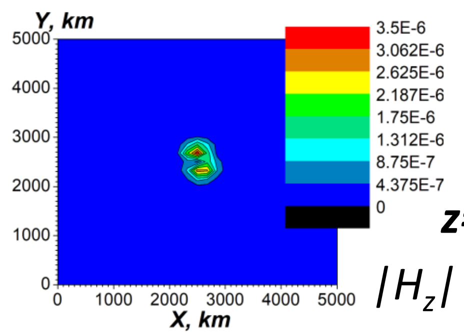

z=60 km

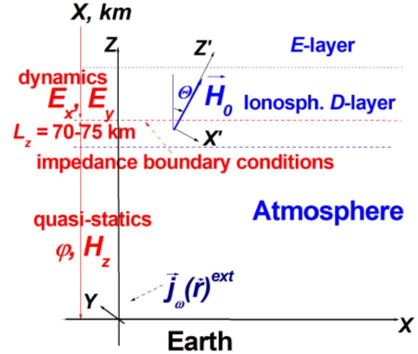

Geometry of the problem

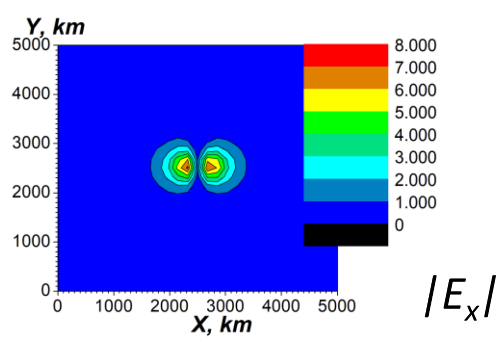

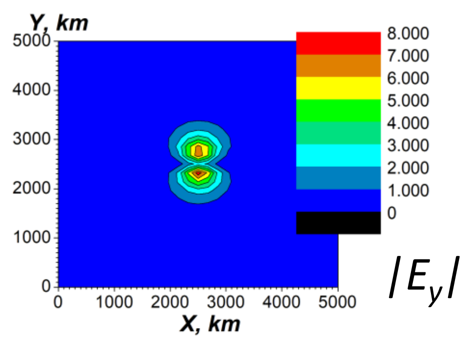

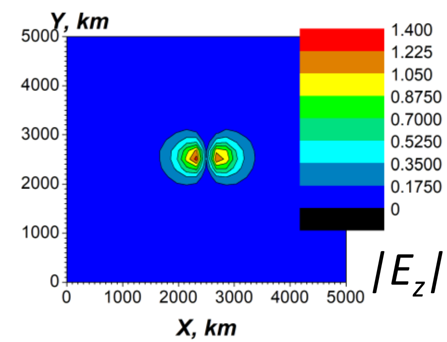

z=400 km

Numerical modelling (night) of penetration of ULF field with given current source: using new integrated dynamic-quasistatic model with inclusion quasimagnetostatic field, lost previously

$$\vec{j}_z^{\,ext} = J_m \exp\left[-\left(\frac{y-0.5L_x}{y_0}\right)^2 - \left(\frac{y-0.5L_x}{y_0^{\;2}}\right)^2 - \left(\frac{z-z_1}{z_0}\right)^2 \right]; \;\; [\vec{E}] = mV/m; \;\; [\vec{H}] = Oe \rightarrow 10^5 \;\; nT;$$

$$J_m = 10^{-7}\, A/m^2; \;\; \theta = 10^\circ; \;\; x_0 = y_0 = 200 \;\; km; \;\; z_1 = 20 \;\; km; \;\; z_0 = 7 \;\; km; \;\; L_x = L_y = 5000 \;\; km; \;\; \boldsymbol{\omega = 2\pi f = 0.001 \;\; s^{-1}}$$

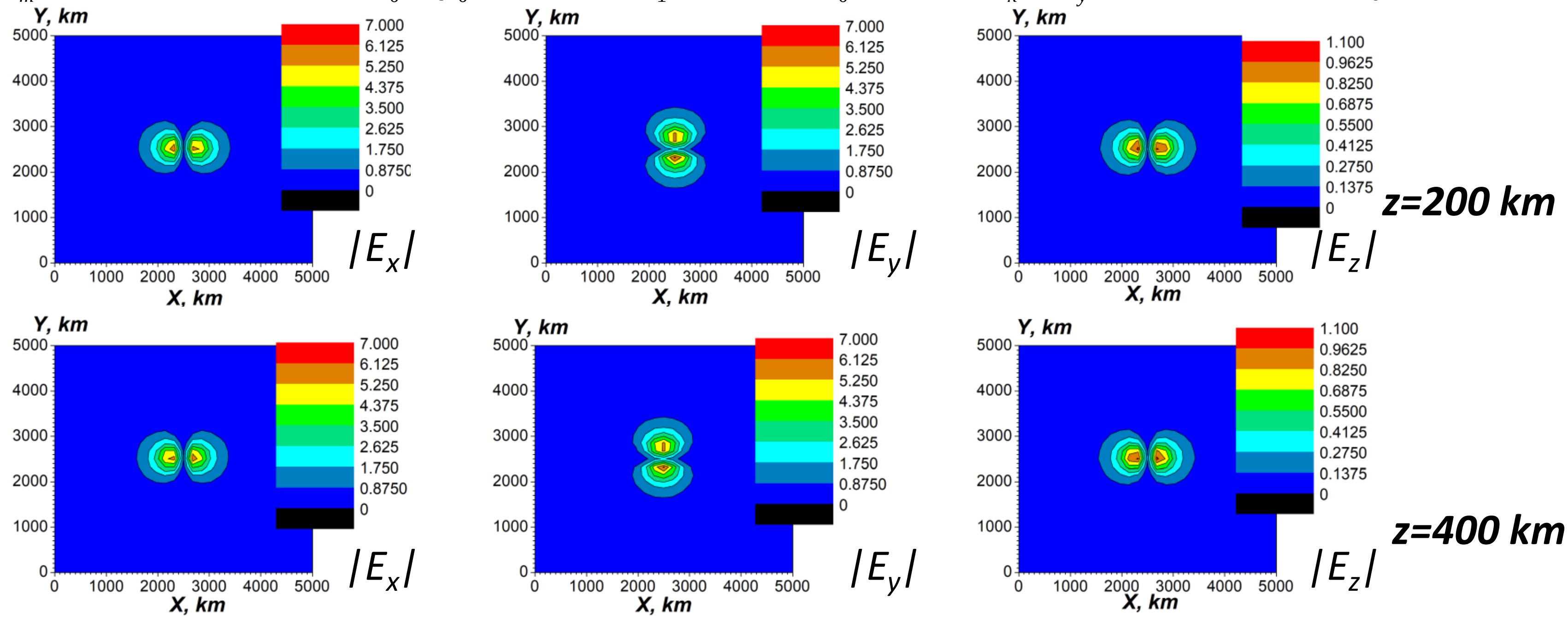

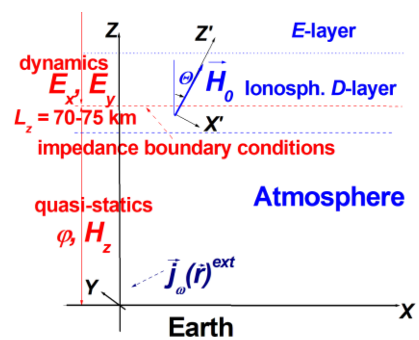

Geometry of the problem

Rapoport, Y.; Reshetnyk, V.; Grytsai, A.; Grimalsky, V.; Liashchuk, O.; Fedorenko, A.; Hayakawa, M.; Krankowski, A.; Błaszkiewicz, L.; Flisek, P.
Spectral Analysis and Information Entropy Approaches to Data of VLF Disturbances in the Waveguide Earth-Ionosphere. Sensors 2022, 22, 8191. https://doi.org/10.3390/s22218191

Spectral analysis and information entropy approaches to data of VLF disturbances in the waveguide Earth-ionosphere (WGEI)

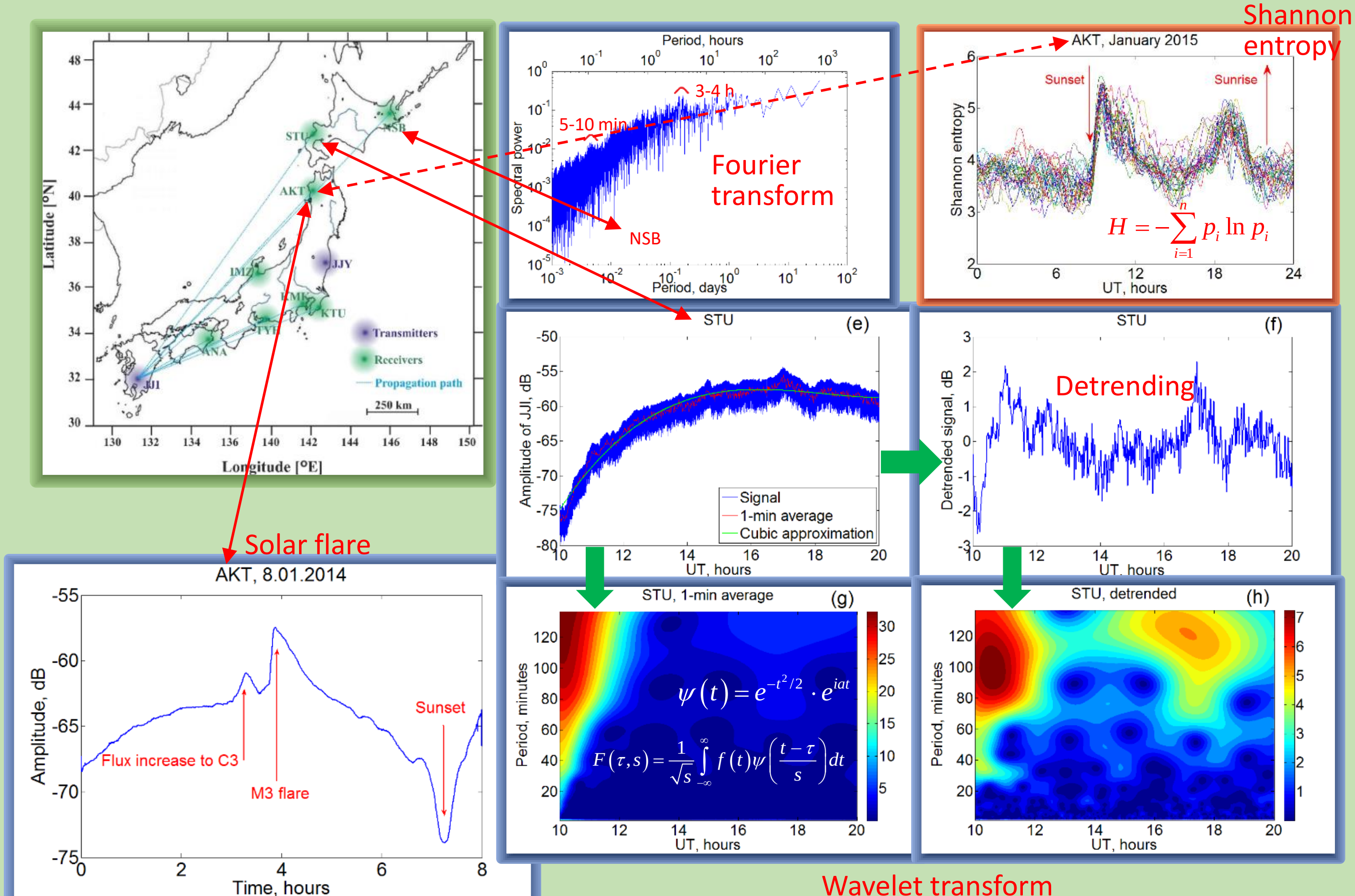

Results

The following variations in the VLF signals propagation in the network of 9 receivers in Japan have been revealed with periods:

5–10 minutes;

20–25 and 60–70 minutes;

3–4 hours;

weekly trend (anthropogenic activity)

Information entropy has been found to show maxima near sunrise and sunset, and the time of these peaks relative to the indicated moments changes with season.

ULF penetration through the system Atmosphere-Ionosphere-Magnetosphere. Limiting pass "Dynamics-quasistatics". New model of VLF electromagnetic waves (EMW) propagation in WGEI. The presence of ULF modulation of the VLF EMW spectrum propagating in WGEI is qualitatively explained. Corresponding models of ULF acoustic-gravity waves (AGW) and their mixing with VLF EMW.

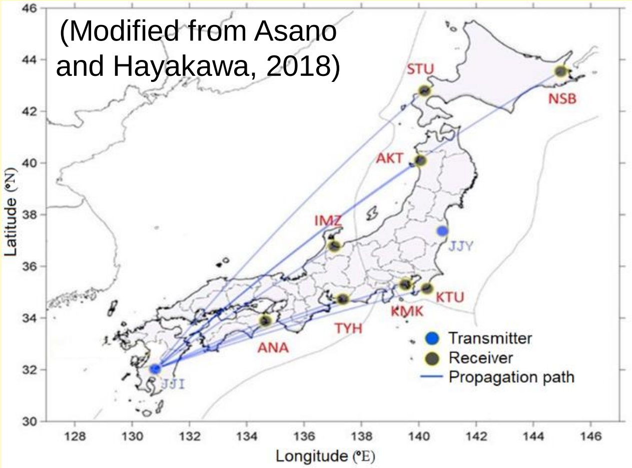

The daily cycle is the most noticeable in the variations of VLF amplitudes

The VLF data contain sharp amplitude decreases which occur in daytime with different repeatability

Daily variations of information entropy are studied with attention to effects of terminator

Influence of other factors is also considered

Information entropy has its maxima near sunrise and sunset, time difference between these peaks and those moments changes with season

Daily cycle of amplitude, different seasons

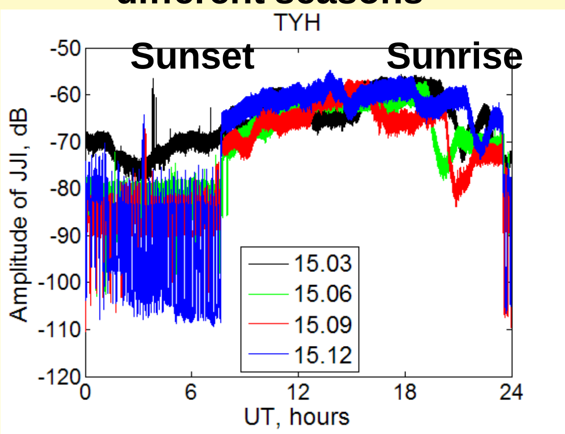

Daily variations of information entropy *H*

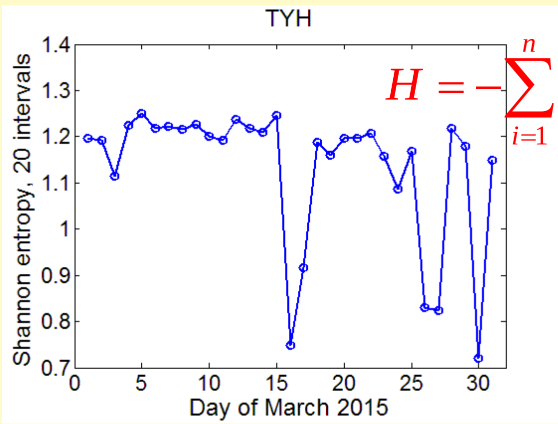

$$H = -\sum_{i=1}^{n} p_i \ln p_i$$

Information entropy: January 2015, NSB station

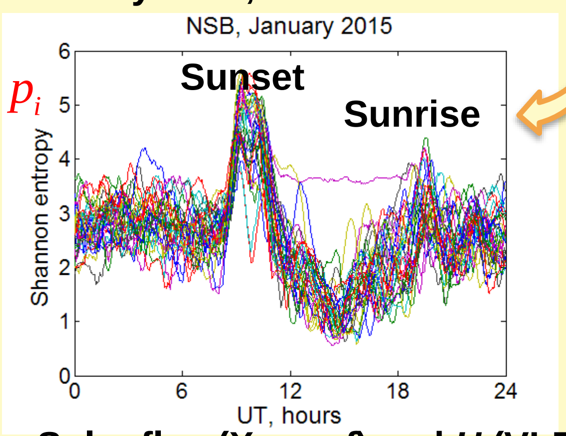

(Japan, data of Prof. M. Hayakawa)

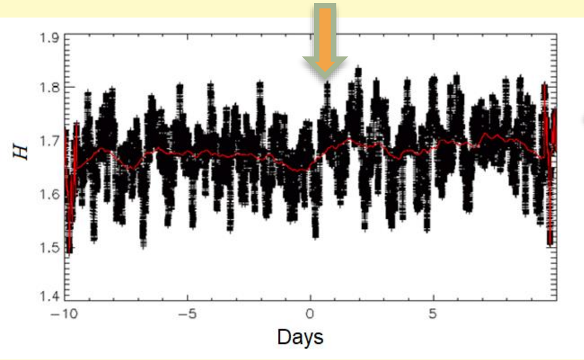

109 earthquakes in 2014–2017: a little decrease of information entropy before an earthquake and its growing after it (method of superimposed epochs)

earthquakes

flares

Solar flux (X-ray, *f*) and *H* (VLF), February 2014

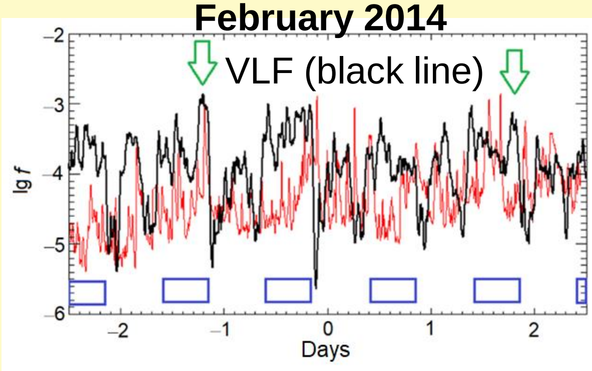

Oscillations are revealed in the VLF spectrum in the waveguide Earth–ionosphere. Their periods: (i) **5–10 min.** – fundamental modes of atmospheric gravity waves (AGW, firstly!); (ii) 20-40 min –AGW; (iii) **2–3 hours** – gravity branch of AGW; also weekly – technogenic trends of ionosphere parameters.

Variations in time

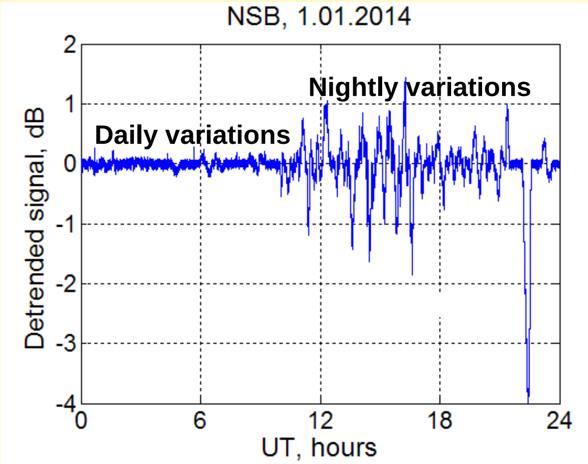

Fourier transform

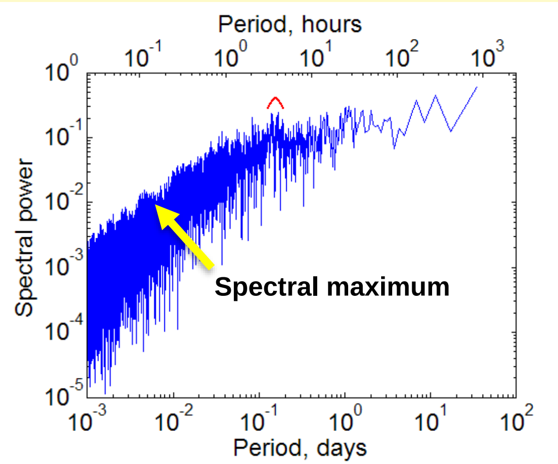

Wavelet transform after detrending

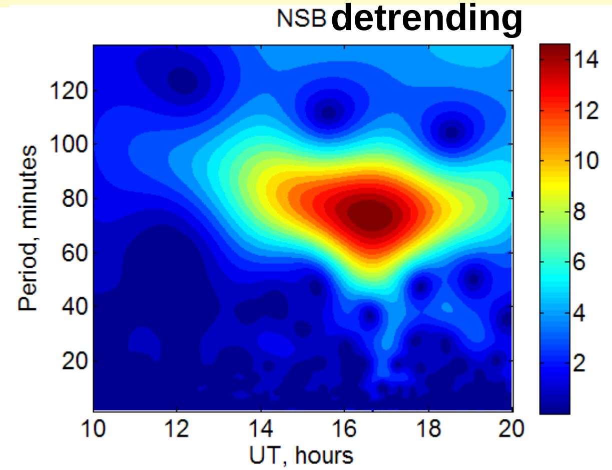

(Japan, data of Prof. M. Hayakawa)

$$\psi(t)=e^{-t^2/2}\cdot e^{iat}$$

VLF amplitude (blue), 1-min average (red), approximation by cubic polynomial (green)

The realization of wavelet transform, March 17, 2015 (example)

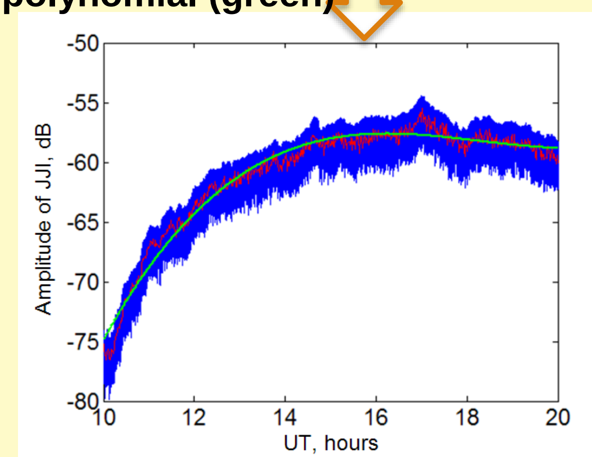

Detrended signal

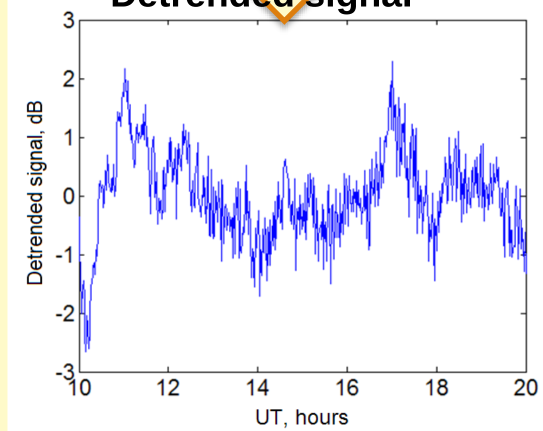

Wavelet transform of the detrended signal

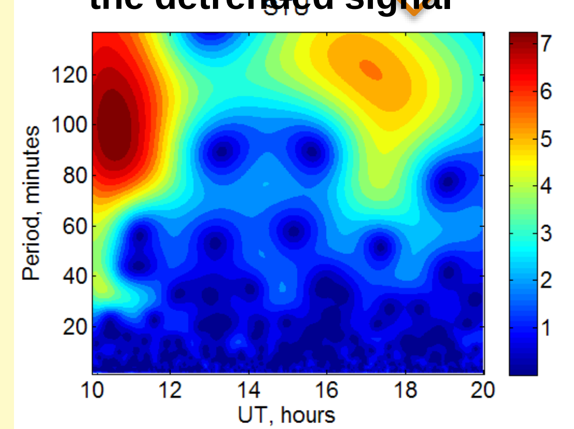

Citation: Rapoport, Y.; Reshetnyk, V.; Grytsai, A.; Grimalsky, V.; Liashchuk, O.; Fedorenko, A.; Hayakawa, M.; Krankowski, A.; Błaszkiewicz, L.; Flisek, P. Spectral Analysis and Information Entropy Approaches to Data of VLF Disturbances in the Waveguide Earth-Ionosphere. *Sensors* **2022**, 22, 8191. https://doi.org/10.3390/s22218191

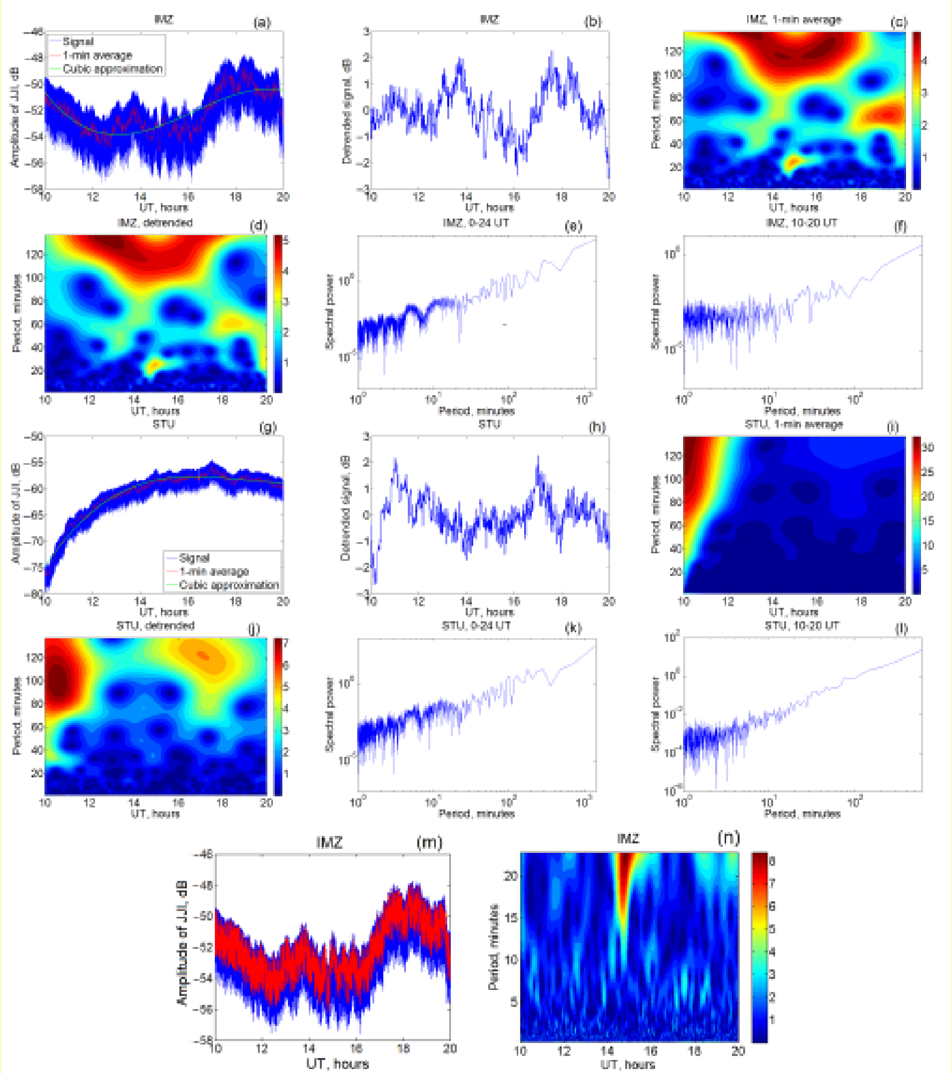

Figure 4. (**a**,**g**) Amplitude of the VLF signal (blue line), its 1-min averaging (red) and trend presented by cubic polynomials (green); (**b**,**h**) detrended signal; (**c**,**i**) wavelet transform after 1-min averaging; (**d**,**j**) wavelet transform after the detrending; (**e**,**f**,**k**,**l**) Fourier spectrum of the VLF signal, the whole day (**e**,**k**) and nighttime period (**f**,**l**) are presented. In all the cases, JJI transmitter signals received at IMZ and STU stations on 17 March 2015 are analyzed; (**m**) measured (blue line) and averaged on 10-s ranges (red line) JJI signal received at IMZ, 17 March 2015; (**n**) wavelet transform of the signal for minute periods.

sensors MDPI

Article

Spectral Analysis and Information Entropy Approaches to Data of VLF Disturbances in the Waveguide Earth-Ionosphere

Yuriy Rapoport [1,2,3,*], Volodymyr Reshetnyk [2], Asen Grytsai [2], Volodymyr Grimalsky [4], Oleksandr Liashchuk [3], Alla Fedorenko [5], Masashi Hayakawa [6], Andrzej Krankowski [1], Leszek Błaszkiewicz [1] and Paweł Flisek [1]

1 Space Radio-Diagnostic Research Centre, University of Warmia and Mazury, 10-720 Olsztyn, Poland
2 Physics Faculty, Taras Shevchenko National University of Kyiv, Kyiv 01033, Ukraine
3 Main Center of Special Monitoring, National Space Facility Control and Tests Center, State Space Agency of Ukraine, 01010 Kyiv, Ukraine
4 Centro de Investigación en Ingeniería y Ciencias Aplicadas, Universidad Autónoma del Estado de Morelos, Cuernavaca 62209, Mexico
5 Space Research Institute National Academy of Sciences of Ukraine and State Space Agency of Ukraine, 01010 Kyiv, Ukraine
6 Hayakawa Institute of Seismo Electromagnetics Co., Ltd. (Hi-SEM), Tokyo 182-0026, Japan
* Correspondence: yuriy.rapoport@uwm.edu.pl

We present the estimations illustrating the possible connection between the periods of oscillations characteristic for AGW and resonant properties of the atmosphere as the media of existence and propagation of AGWs. A detailed substantiation of this possibility of resonant modulation of VLF spectra by AGW frequencies is presented in Appendix A. For the convenience of readers, here we very briefly outline the essence of what is presented in Appendix A, namely: (1) interaction between AGW existing in the atmosphere and VLF EMW propagating in the WGEI can be connected with the generation in the ionosphere of the currents on the combinations $\omega_{VLF} \pm \omega_{AGW}$ of the frequencies ω_{VLF} of VLF EMWs and ω_{AGW} of AGWs. Such the current can be caused by two factors (see relations (A5), (A6) in Appendix A): (a) dragging of charged particles by means of AGWs against the background of ionospheric plasma with disturbances of charged particle concentration caused by VLF EMW; (b) motion of plasma particles with frequency of VLF EMW on the background of slowly varying plasma concentration, caused by AGW in the atmosphere–ionosphere; (2) AGW as global oscillations in the atmosphere–ionosphere are excited resonantly, and therefore relatively very efficiently, as the so-called reactive, or evanescent, modes [20,55–59]; an influence of the AGW packets containing such modes on the stable and unstable ionosphere has been investigated in [19,60] and [20,61], respectively. The estimation presented below would not cover comprehensively the all complex processes of the VLF modulation by AGW, outlined above. In the present paper, we restrict ourselves only with the demonstration of the fact that the obtained spectra of the modulation of VLF EMWs propagating in WGEI are quite compatible with the conditions of the resonant excitation of the global AGW modes. Then, we suppose that such resonant AGW mode excitations may be the reason of the most remarkable components of the revealed VLF spectra. Two main resonant reactive AGW modes [20,55–59] are the Lamb waves for which

$$\lambda_y = c\tau; \quad k_y \equiv 2\pi/\lambda_y; \quad c^2 = \gamma g H; \quad H = k_B T/mg \tag{9}$$

and Brunt–Väisälä oscillations with frequency

$$\omega \equiv \omega_{AGW} = \omega_B; \quad \omega_B^2 = [(\gamma-1)/\gamma](g/H) \tag{10}$$

In Equations (9) and (10), τ, k_y and λ_y are AGW period, wavenumber in horizontal direction and corresponding wavelength, respectively; c, g, H and γ are atmospheric sound speed, free-fall acceleration, atmospheric scale height and the adiabatic constant for the atmosphere; k_B, T and m are the Boltzmann constant, temperature of the (neutral) atmosphere and average mass of the atmospheric particles. Note that the temperature in the lower part of the atmosphere ($z \le 100$ km) does not change, in particular with altitude, remarkably compared to one in the thermosphere, respectively; the local approximation for the AGW field in the atmosphere can be used for the evaluations [62]. Respectively, it is supposed that the AGW velocity components $V_{y,z}$ are proportional to $\exp[i(\omega t - k_y y - K_z z)]$; here, $K_z = i/2H + k_z$, where the first term is connected with the presence of atmospheric stratification [62,63], $k_z = k_z' + ik_z''$ is the effective vertical wavenumber of AGW with real and imaginary parts equal to k_z' and k_z'', respectively. For the propagating modes (in vertical direction), $k_z'' = 0$ [63], while for the resonant reactive modes (9), (10), $k_z'' \neq 0$ [19,56,58–60]. In spite of the evanescent character of these modes, their impact on the ionosphere and VLF waves perturbations may be important in the case of the sources, distributed by the altitudes in the atmosphere–ionosphere in the wide amplitude range Δz; Δz is on the order of a few dozens of kilometres, namely $\Delta z \sim 20$ km for the strongest tropical cyclones [64,65] and for the sources forming before the strongest earthquakes [66]; seismogenic sources forming after the strongest earthquakes are powerful enough to provide the covering by the corresponding excited waves all the atmospheric altitude ranges up to the ionosphere [67]. Accounting for this, we will stress in our estimations on the most effectively excited global atmospheric Brunt–Väisälä oscillations and Lamb waves, in spite of their reactive character with the characteristic scale of evanescent decrease with the altitude of order $|k_z''|^{-1} \sim H$. Consider these evaluations for the several characteristic spectrum components revealed during the data processing described above in the present Section 3.

The spectra maximum with the period $\tau \sim 3$ h $\sim 10^4$ s, accounting for that [63], $c \sim 0.3$ km/s may correspond, by the order of value, to the excitation of the Lamb wave with the half wavelength of order of 1500 km ($\lambda_y = c\tau/2$, compare with relation (9)), which corresponds to the characteristic dimension of the size of the horizontal projection of the terminator, see Figure 4n and [68]. Earthquake [18,69] or tropical cyclone [43] sources with the horizontal sizes (300–1000) km may excite the Lamb waves with the corresponding wavelengths (see Equation (9) and Appendix A) and the periods of order of (20–60) min (see Figures 4c–e,k and 7). Then, the oscillations with periods $\tau \sim$6–7 min, presented in the VLF spectra (Figure 7), are probably excited global atmospheric Brunt–Väisälä oscillations (see Equation (10) and Appendix A, relations (A20)). Note also that the periods of the order of few minutes revealed in the VLF spectra (see Figures 4k,n and 7) may characterise the AGW modes in the opened waveguide Earth–Thermosphere [70]. In accordance with the dispersion equation (based on the isothermal approximation [63] presented in Appendix A in the first line from the relations (A17), the dispersion of the AGW branch mode of waveguide Earth–Thermosphere is approximately:

$$\omega/\omega_a \sim \sqrt{1+\left[(2H)^2 \cdot \left(k_y^2 + k_z^2\right)\right]}; \; \omega_a \equiv c_a/2 \cdot H; \; k_z \sim \pi/L \tag{11}$$

In (11), $L \sim 100$ km is the effective width of the "Earth-Thermosphere" waveguide of the AGW. Using relation (11) and putting, for the rough estimations $H \sim 8$ km [63] and $k_y \sim k_z$, yields $\tau = 2\pi/\omega \sim 4$ min. By the order of value, such evaluations correspond to the similar theoretical results for AGW period presented in [71] and to the periods revealed in the spectra of VLF (see Figure 4n).

The more detailed analysis would be necessary to reveal the VLF modulation in WGEI by the strongly excited double resonant Brunt–Väisälä–Lamb oscillations [59], see relation (A21). This will be a subject of the next paper(s).

Note also that the oscillations with periods (1–2) min., which are the most pronounced among the AGW oscillations revealed in [54] from the spectra of VLF waves on the Germany–Serbia path, reflected from the upper boundary of the WGEI, are also presented in the spectra revealed from our data obtained as a result of the processing VLF data from the Japan paths (Figure 4n). In distinction to the data presented in [54], our data oscillations with periods (1–2) min are relatively weakly pronounced (Figure 4n).

VLF disturbance with ULF modulation in the Waveguide Earth-Ionosphere (WGEI)

AGW: For propagation upward and wave field $\sim e^{i\omega t}$ →

In the absence of losses → $\vec{u} \sim e^{i(\omega t - k_z' z)} e^{k_z'' z}; \; k_z'' = \dfrac{1}{2H} + \delta k_z''$

If $\delta k_z'' < 0$ → evanescent (reactive) AGW modes

Main resonant reactive AGW modes → Lamb waves:

$$\lambda_y = c\tau; \; k_y = 2\pi / \lambda_y; \; c^2 = \gamma g H; \; H = k_B T / mg; \; \tau = 2\pi / \omega$$

$$\omega = \omega_B; \; \omega_B^2 = [(\gamma - 1)/\gamma](g/H)$$

$$\tau \sim 3 \; h \sim 10^3 s; \; c \sim 0.3 \; km/s; \; \lambda / 2 \sim 1500 \; km \rightarrow$$

Corresponds to the size horizontal projection of the terminator;

Tropical cyclones or earthquake with the horizontal sizes ~(300-1000 km) may exite Lamb waves with the periods τ~(20-60) min; the oscillations with periods τ~(6-7) min.

The dispersion of AGW mode of WGEI:

$$\omega / \omega_a \sim \sqrt{1 + (2H)^2 (k_y^2 + k_z^2)}; \; \omega_a = c_a / 2H; \; k_z \sim \pi / L; \; L \sim 100 \; km; \; H \sim 8km;$$

$$If \;\; k_y \sim k_z \rightarrow \; \tau = 2\pi / \omega \sim 4 \; \text{min}$$

Influence of AGW on the ionosphere and mixing VLF EMW + ULF AGW

$$N_l m_l [\frac{\partial \vec{V}_l}{\partial t} + (\vec{V}_l \vec{\nabla})\vec{V}_l] - N_l \frac{q_l}{c}[\vec{V}_l \times \vec{H}_0] + \nu_l q_l N_l \vec{V}_l = N_l q_l m_l \vec{E}_{l\ eff}$$

$$l = i; e;\ \ \vec{E}_{l\ eff} = \vec{E} + \frac{\nu_l}{q_l}\vec{V}_{AGW}$$

$$\frac{\partial N_l}{\partial t} + \vec{\nabla}(N_l \vec{V}_l) = 0$$

$$N_l = N_{e0} + N'_{AGW} + N'_{VLF} \equiv N_{e0} + N'_{AGW\,00} e^{j\omega_{AGW}t - jk_{AGW}y} + N'_{VLF\,00} e^{j\omega_{VLF}t - jk_{VLF}y}$$

$$\vec{V}_{AGW} = \vec{V}_{AGW\,00} e^{j\omega_{AGW}t - jk_{AGW}y}$$

$$\vec{j}^{(VLF+AGW)} = [\sum_{l=i;e} q_l N_l \vec{V}_l]^{(VLF+AGW)}$$

$$\vec{E}_{VLF} = \vec{E}_{VLF\,00} e^{j\omega_{VLF}t - jk_{VLF}y};\ \ \vec{E}_{VLF\,00} = \vec{A}_1 f_E(z)$$

$$\hat{\varepsilon} = \hat{I} + \frac{4\pi\hat{\sigma}}{i\omega};\ \ \hat{\sigma} = \hat{\sigma}_i + \hat{\sigma}_e;\ \ \vec{V}_{i,e} = \hat{\mu}_{i,e}\vec{E}_{eff};\ \ \hat{\mu}_l = \frac{1}{q_l N_{0l}}\hat{\sigma}_l$$

$$E^{(AGW+VLF)} \square\ A_l^{(AGW+VLF)} f_E e^{j(\omega_{VLF}+\omega_{AGW})t - j(k_{VLF}+k_{AGW})y}$$

$$|A_l^{(AGW+VLF)}| \square |\vec{E}_{VLF\,00}||\vec{V}_{AGW\,00}| \square |A_1||\vec{V}_{AGW\,00}|$$

Excitation of oscillation in coupled Schumann Resonator - Ionospheric Alfven Resonator (SR-IAR) are possible!

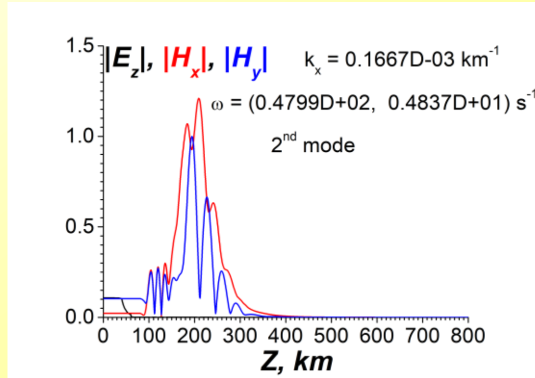

$\omega = \omega_{SR}$

Resonant SR-IAR frequency ω comparatively to standard Schumann Resonance frequency $\omega_{SR} \sim cR_E^{-1}$

$\omega > \omega_{SR}$

$\omega < \omega_{SR}$

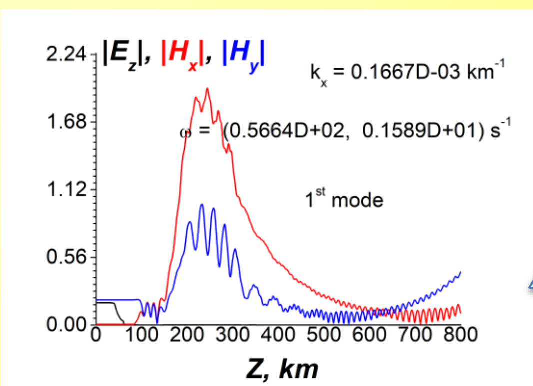

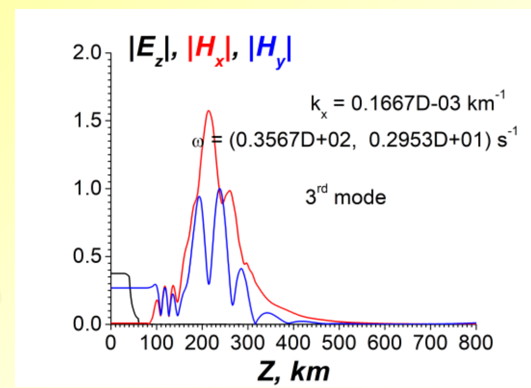

Important: (1) $k_x = \mathrm{Re}(k_x) \approx R_E^{-1}\ [\mathrm{Im}(k_x) = 0]$; (2) $\omega = \mathrm{Re}(\omega) + i\,\mathrm{Im}(\omega)\ (\vec{E}, \vec{H} \sim e^{i(\omega t - k_x x)})$;
(3) But, when the field of the modes is determined, we put $\mathrm{Im}(\omega) = 0$ (Vainstein L.A. Open Resonators and Open Waveguides, Sov. Radio, Moscow, 1966)

Waveguide Earth-Ionosphere and Ionosphere Alfven resonator

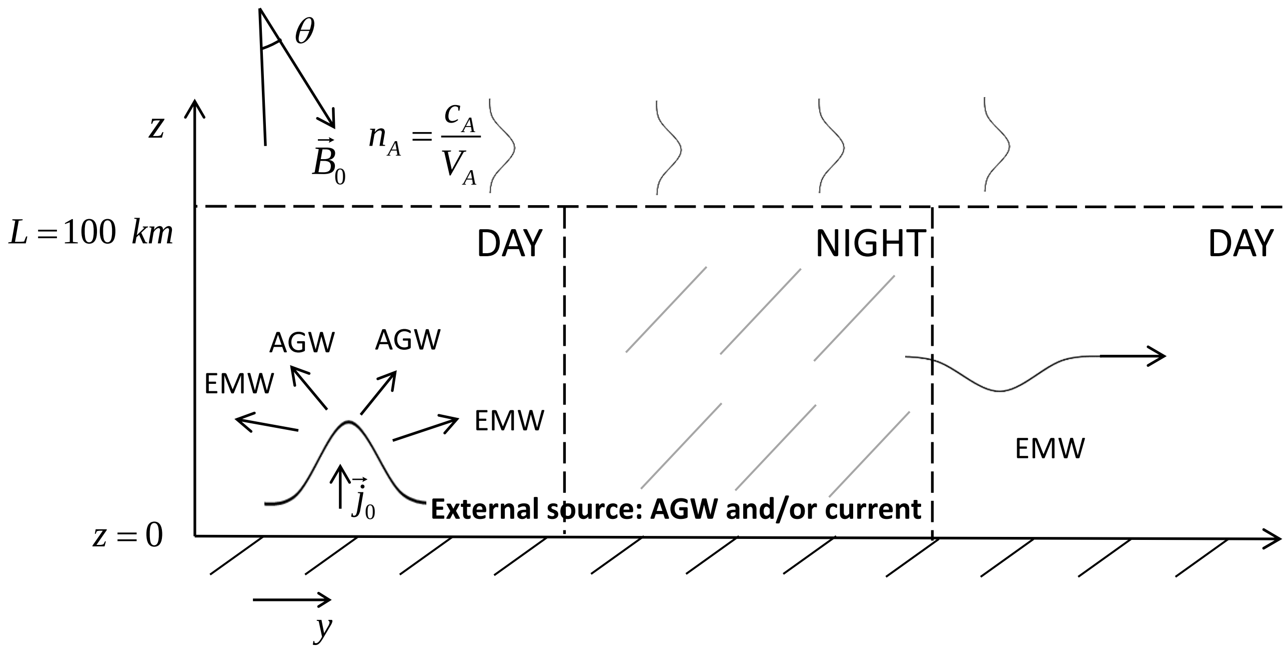

Coupling in the system (Earth)-Atmosphere-Ionosphere-Magnetosphere (LEAIM)

[3D coupled Perkins E_s instability. T. Yokogama et al. VGR 114, A0 3308 1-16, 2009]

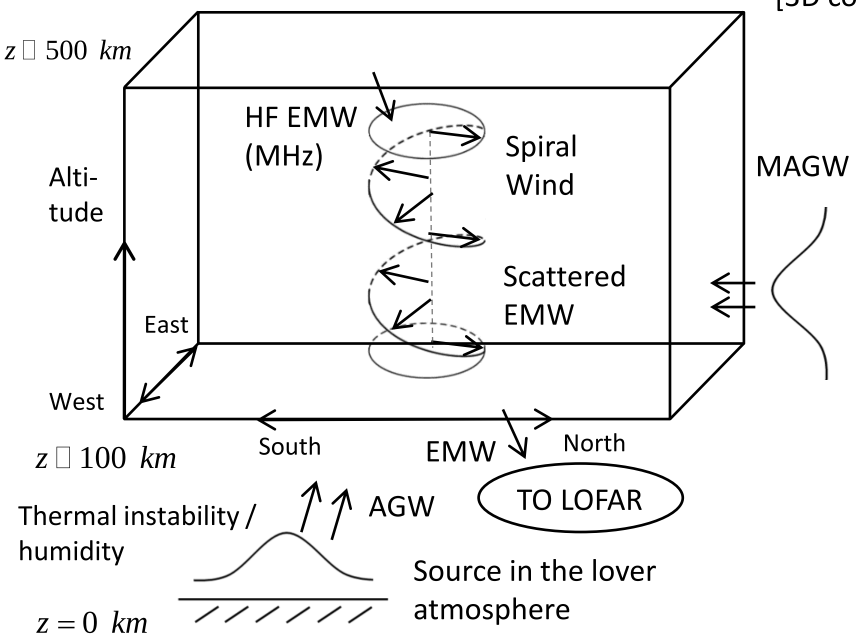

Perkins instability $\gamma_P = \dfrac{\left|\vec{E}_0 + \vec{V}^F \times \vec{B}\right| \cos I}{B_H} \sin(\theta\alpha)\sin(\alpha)$

E_s-layer instability (sporadic E_s) $\gamma_E = \dfrac{V_x^E \cos I}{H_0 \rho_i}\left(\dfrac{\Sigma_H^{E_s}}{\Sigma_P^{E_s} + \Sigma_P^E + \Sigma_P^F}\sin(\alpha)\cos(\alpha) - 1\right)$

$\rho_i = \upsilon_{in}\Omega_i$

$\Sigma_{H,P}$ - field line integrated Hall and Pederson conductivities, respectively

Under the nighttime – Σ_H is provided by E_s layer

Σ_P is provided by F region → E_s and F (Perkins) instabilities do interact with each other

$\vec{E}_0$ and $\vec{B}$ – background electric filed and geomagnetic field

θ - angle between the total effective electric filed $\vec{E}_0 + \vec{V}^F \times \vec{B}$ and the east direction;

I - magnetic inclination angle;

α - angle between the direction normal to the frontal structure and east direction;

H - atmosphere scale hight

$H_U = \left(\dfrac{1}{U_x^E}\dfrac{\partial U_x^E}{\partial z}\right)^{-1}$ - scale height of vert. shear U_x^E

$$\gamma_P^C = \gamma_P + \Delta\gamma_{E\to F};\ \gamma_E^C = \gamma_E + \Delta\gamma_{F\to E}$$

Coupled Perkins-E_s instability

At the same range of altitudes where TEC and different structures in ionospheric E-F structures are formed E [characterictic] (10-100) mV/m **(!)**

AGW or MAGW seeding factor for E_s-F instability

Travelling Ionospheric Disturbances (TIDs) [Ratcliffe 1956; Rishbeth, Garcott 1969; Hooke 1968; Francis 1974; Clark 1971; Yeh, Lin 1974, 1972; Shiokawa2003; Koval 2018; Rapoport 2004; 2017; Vadas 2005; Matcheva 2001]

AGW – gravity branch, approximately

$$\begin{pmatrix} u \\ v' \\ \omega' \\ p' \\ T' \end{pmatrix}(x,y,z) = \begin{pmatrix} \delta u(z) \\ \delta v'(z) \\ \delta\omega'(z) \\ \delta p'(z) \\ \delta T'(z) \end{pmatrix} \exp[i(k_x x + k_y y - \omega_0 t)]$$

$$\omega_0^2 \ll N;\; H^{(*)} = (-\frac{1}{\rho_0}\frac{\partial \rho_0}{\partial z})^{-1};\; H = (-\frac{1}{p_0}\frac{\partial p_0}{\partial z})^{-1};\; (H - H^{(*)})/H^{(*)} \ll 1;$$

$\Gamma = (\frac{\partial \tau_0}{\partial z} + \frac{g}{c_p})$ – static stability coeff.; P_r – Prandtl number; μ – mol. din. vis.

$\chi = c_p \mu / P_r$ – molecular thermal heat conduct; $k_z \gg \max(k_x, k_y)$

Use qualitively ωxB approximation

$$\frac{\partial^2 \tilde{\omega}}{\partial u^2} + k_z^2 \tilde{\omega}(z) = 0;\; \tilde{\omega}(z) = \delta\omega(z)\exp(-\int dz / H^*)$$

$$\vec{\nabla}\cdot\vec{V}' - \frac{\omega'}{H^*} = 0; \quad [\frac{\partial}{\partial t} + u_0\frac{\partial}{\partial x} - \frac{1}{\rho_0}\frac{\partial}{\partial z}\mu\frac{\partial}{\partial z}](u', v') = -\frac{1}{\rho_0}\frac{\partial \rho'}{\partial(x,y)}$$

$$k_z^2 = \frac{k_n^2 N^2}{\tilde{\omega}(\tilde{\omega} + i\beta)} - \frac{1}{4H^{*2}}[1 - 2\frac{dH^*}{dz}]$$

$N^2 = (gr/\tau_0)$ – buoyancy frequency

$$[\frac{\partial}{\partial t} + u_0\frac{\partial}{\partial x} - \frac{1}{\rho_0 P_r}\frac{\partial}{\partial z}\mu\frac{\partial}{\partial z}]T' + \Gamma\omega' = 0;\; \frac{\partial}{\partial z}(\frac{p'}{\rho_0}) = \frac{T'R}{H}$$

$$\tilde{\omega}=\omega_r+i\omega_i;\ \ \omega_r=-\mathrm{Im}[\frac{1}{u'}(\frac{\partial}{\partial t}+u_0\frac{\partial}{\partial x}-\nu\frac{\partial^2}{\partial z^2})u']=\tilde{\omega}_0+2k_{zr}\nu(\frac{1}{2H^*}-k_{zi})$$

$$\omega_i=\mathrm{Re}[\frac{1}{u'}(\frac{\partial}{\partial t}+u_0\frac{\partial}{\partial x}-\nu\frac{\partial^2}{\partial z^2})u']=\nu[k_{zr}^2-(\frac{1}{2H^*}-k_{zi})^2]$$

$$\beta=-\mathrm{Re}[\frac{1}{\Gamma}(\frac{1}{P_r}-1)\nu\frac{\partial^2}{\partial z^2})T']=(\frac{1}{P_r}-1)\nu[k_{zr}^2-(\frac{1}{2H^*}-k_{zi})^2]$$

$\tilde{\omega}_0=\omega_0-u_0k_x$ - internal wave frequency; u_0- wind velocity

$\nu=\mu/\rho_0$ - kinetic viscosity; wave-like solution (ωxB)

$$\tilde{\omega}(z)=\Delta\omega(z_0)[\frac{k_{zr}(z_0)}{k_{zr}(z)}]^{1/2}\exp[-\int_0^z k_{zi}dz]\exp[i\int_{z_0}^z k_{zr}dz]$$

$\Delta\omega(z_0)$ - amplitude of reference altitude

$$\omega'(x,y,z,t)=\Delta\omega(z)\cos\varphi;\quad \Delta\omega=\Delta\omega(z_0)(\frac{k_{zr}(z_0)}{k_{zr}(z)})^{1/2}\exp[\int_{z_0}^z(\frac{1}{2H^*}-k_{zi})dz]$$

$$\varphi=k_xx+k_yy+\int_{z_0}^z k_{zr}dz-\omega_0t$$

$$T'(x,y,z,t)=\frac{\Gamma}{\omega_r}\Delta W(z)\cos\theta\cos(\varphi-\frac{\pi}{2}-\theta)$$

$$p'(x,y,z,t)=-\frac{\omega_rk_{zr}}{k_h^2}\Delta W(1-\frac{\omega_i}{\omega_r}(\frac{k_{zi}}{k_{zr}}+\frac{1}{2H^*k_{zr}}))\frac{\cos(\varphi-\theta')}{\cos\theta'}$$

$$\tan\theta=\frac{1}{p_r}\frac{\omega_i}{\omega_r};\quad \tan\theta'=(\frac{\omega_i}{\omega_r}+\frac{k_{zi}}{k_{zr}}+\frac{1}{2H^*k_{zr}})[1-\frac{\omega_i}{\omega_r}(\frac{k_{zi}}{k_{zr}}+\frac{1}{2H^*k_{zr}})^{-1}]$$

Equation and solution for electron concentration

$$\frac{\partial N_e}{\partial t} + \vec{\nabla}(N\vec{V}_e) = P - L; \qquad L = \frac{\alpha\beta N_e^2}{(\beta + \alpha N_e)} = L_0 + L'$$

Linearization:

$$L_0 \approx \alpha \frac{N_{e0}^2 + \left\langle N_e'^2 \right\rangle}{1 + \frac{\alpha}{\beta} N_{e0}}; \;\; L' \approx \frac{N_{e0}^2 + \left\langle N_e'^2 \right\rangle}{1 + \frac{\alpha}{\beta} N_{e0}} [\frac{2N_{e0}}{N_{e0}^2 + \left\langle N_e'^2 \right\rangle} - \frac{(\alpha / \beta)}{1 + \frac{\alpha}{\beta} N_{e0}}] N_e' = L_1 N_e'$$

$$\frac{\partial N_e'}{\partial t} + \vec{\nabla}(N_{e0}\vec{V}_{e0} + N_e' \vec{V}_e') = P' - L / N_e'$$ - perturbed equation

$$\vec{\nabla}(N_{e0}\vec{V}_{e0} + \left\langle N_e' \vec{V}_e' \right\rangle) = P_0 - L_0$$

In the absence of background wind $\vec{V}_{e0} = -\frac{2k_B T_p}{m_i \nu_{in0}} [(\frac{\vec{\nabla} T_p}{T_p} + \frac{\vec{\nabla} N_e}{N_e} + \frac{\vec{l}_z}{H_p}) \vec{l}_B] \vec{l}_B$

T_B - plasma temperature; H_p - plasma scale high; $\vec{l}_z = -\vec{g} / |\vec{g}|; \; \vec{l}_B = -\vec{B} / |\vec{B}|;$

$\vec{U}_l' = \vec{U}_c' + \vec{U}_d';$ "c" and "d" - collision and diffusion, respectively.

For the collision part of drift: $\vec{U}_c = \frac{1}{1+\eta^2} [\eta^2 \vec{U}_n' + \eta \vec{U}_n' \times \vec{l}_B + (\vec{U}_n' \cdot \vec{l}_B) \vec{l}_B]$

$\eta = \nu_{in} / \omega_B;$ $\vec{U}_n'$ - neutral wind velocity; in F region; $\eta \ll 1,$ $\vec{U}_c' \approx (\vec{U}_n' \cdot \vec{l}_B) \vec{l}_B$

Suppose charge of ion production P’ induced by GWs is negligible

$$[\frac{\partial}{\partial t}+(L_1+(\vec{\nabla}\vec{U}_{d_0})+(\vec{U}_{d_0}\vec{\nabla})]N'_e+\vec{\nabla}N_{e0}\vec{V}'_e=0$$

Analytical accounting for chemistry and diffusion effects

$$\hat{D}=[\frac{\partial}{\partial t}+(L_1+(\vec{\nabla}\vec{U}_{d_0})+(\vec{U}_{d_0}\vec{\nabla})]$$

$$\Omega=i\frac{1}{N'_e}\hat{D}N'_e$$

$$N'_e(x,y,z,t)=N_{e0}\frac{(\vec{U}'_n\cdot\vec{l}_B)}{\Omega}[\vec{k}_r\vec{l}_B-i(\frac{1}{N_{e0}}\frac{\partial N_{e0}}{\partial z}+\frac{1}{2H^*}-k_{zi})(\vec{l}_B\vec{l}_z)]$$

$$\Omega_r \approx \omega_0-\vec{k}_r\vec{U}_{d_0};\ \Omega_i \approx L_1+\vec{\nabla}\vec{U}_{d_0}-(\vec{k}_i+\frac{1}{N_{e0}}\vec{\nabla}N_{e0}-\frac{1}{N_{e0}}\vec{\nabla}N_{e0})\vec{U}_{d_0}$$

$$\Omega_i \approx L_1+\vec{\nabla}\vec{U}_{d_0}-(\vec{k}_i+\frac{1}{N_0}\vec{\nabla}N_0-\frac{1}{N_{e0}}\vec{\nabla}N_{e0})\vec{U}_{d_0};$$ N_0 - background atmospheric concentration

Nonlinear equation for electron concentration.

$$\frac{\partial N_e}{\partial t}+\vec{\nabla}\{-N_e\sigma[\frac{\vec{\nabla}N_e}{N_e}+\frac{\vec{\nabla}T_p}{T_p}+\frac{\vec{l}_z}{H_p})\vec{l}_B+N_e(\vec{V}_n\vec{l}_B)\vec{l}_B\}=\frac{\alpha\beta N_e^2}{(\beta+\alpha N_e)}$$

$$\sigma=\frac{2kT_p}{m_i\nu_{in0}}$$

Generalization of the equation for TID concentration to the case of presence of vertical and horizontal wind and recombination / photochemistry process

$$n_i \square n_e$$

$$\frac{\partial n_i}{\partial t} = \frac{\partial}{\partial z}(D_a \sin^2 I(\frac{\partial n_i}{\partial z} + \frac{n_i}{T_p}\frac{\partial T_p}{\partial z} + \frac{n_i}{H_p}) - \omega n_i] - \beta n_i + q$$

$z = (200 - 500)\ km;$ For the main ion O+ → Production $Q_i = q;$; recombination $L_i = \beta N_i$

$\omega = (V_{n\square})_z + (V_{i1})_z;\ (\omega_{nH})_z - [wind + AGW];\ (V_{iI})_z - EM\ \ drift$

$$\varphi = k_x x + k_y y + \int_{z_0}^{z} k_{zr} dz - \omega_0 t; \qquad \Delta W_{nz} = \Delta W_n(z_0)(\frac{k_{zr}(z_0)}{k_z(z_0)})^{1/2}$$

$$\vec{V}_{AGW} = \square W_n(z)\exp(i\varphi)[\alpha_{Vxz}, \alpha_{Vyz}, 1];\ T_P = T_{0P} + \alpha_{Tz} \square W_n(z)\exp(i\varphi)$$

$$\vec{V}_i^{\perp} = -(c / H^2)[\vec{H} \times \vec{E}];$$

Linearization: $n_i' = \alpha_{n_i\omega} \square W_n(z)\exp(i\varphi)$

$$\alpha_{n_i\omega} = \alpha_{n_i\omega}(I, k_{zr,} (V_{nn})_z, ...)$$

Note! TID vertical profile has Δz~150 km

Optical thickness for so-called this scattering screen

$$f \square 4 \cdot 10^7 Hz$$

$$\lambda \square 10^{-2} km$$

$$L \square 150 \cdot \frac{2\pi}{\lambda} \square 10^5$$

$L_{opt} = k_{EMWz} \Delta z \square 10^5 \square\ 1$ → Opposite to “thin screen”

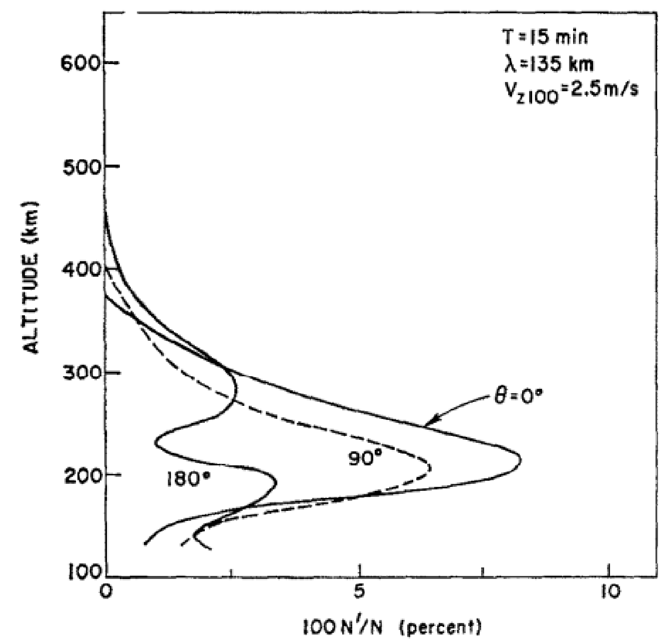

Perturbed concentration profile; AGW, *T*=15 min [Davis. JASTP 1973]

Complex geometrical optics: real rays; $\vec{V}_{g\ eff} = \mathrm{Re}(\vec{V}_g)$

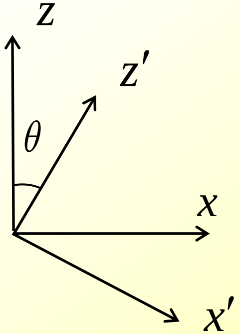

$$\hat{\varepsilon}' = \begin{pmatrix} \varepsilon_1 & ig & 0 \\ -ig & \varepsilon_1 & 0 \\ 0 & 0 & \varepsilon_3 \end{pmatrix}$$

$$\vec{E} \sim \exp(i\omega t)\exp(-i\vec{k}\vec{r})$$

Also:

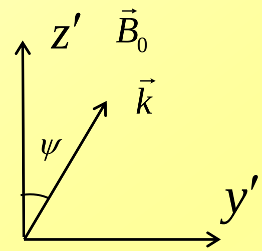

[- frame]

To get dispersion equation we use (x', y', z')

$$n^2 \equiv k^2 / k_0^2;\ \ k_0 \equiv \omega / c;\ \ ; n_j = k_j / k_0;\ \ \vec{\nabla}(\vec{\nabla}\vec{E}) - \Delta\vec{E} - k_0^2 \hat{\varepsilon}\vec{E} = 0$$

$$n^2 = n_1^2 + n_2^2 + n_3^2;\ \ n^2 \sin^2\psi = n_1^2 + n_2^2;\ \ n^2\cos^2\psi = n_3^2$$

Similarly for *y,z*

$$\frac{dx}{dt} = V_1 = -\mathrm{Re}(\frac{D_{k_x}}{D_\omega});\ \ \frac{d\omega}{dt} = -\frac{D_t}{D_\omega}$$

$$(h^2 - \varepsilon_1)E_1 - igE_2 = 0$$

$$igE_1 + (n_3^2 - \varepsilon_1)E_2 - n_2 n_3 E_3 = 0 \ \Rightarrow$$

$$-n_2 n_3 E_2 + (n_1^2 - \varepsilon_3)E_2 = 0$$

Dispersion equation: $D = 0;$

Local basis: $\vec{l}_{V_z} \parallel \vec{V} \Rightarrow \vec{l}_{V_z} = (\frac{V_1}{V}, \frac{V_2}{V}, \frac{V_3}{V}) = (r_1, r_2, r_3)$

$$k_{x,y,z} - complex;\ \ \vec{V}_{g\ eff} = \mathrm{Re}(\vec{V}_g)$$

$$D = k^2c^2 - \omega^2 + \omega_p^2 F(\vec{r}, \vec{k}, \omega) = 0;\ \ F = 1 + \frac{i\nu}{\omega} + W^2[\cos^2\psi + \frac{\sin^2\psi}{2(1-u)}] - \tilde{\Delta}$$

$$\tilde{\Delta} = \{W^2\cos^2\psi + [\frac{W^2\sin^2\psi}{2(1-u)}]^2\}^{1/2};\ \ u = \frac{\omega_P^2}{\omega^2};\ \ W = \frac{\omega_B}{\omega} \ll 1$$

$$an^4 - bn^2 + d = 0;\ \ a \equiv \varepsilon_1 \sin^2\psi + \varepsilon_3\cos^2\psi;\ \ b = \varepsilon_1\varepsilon_3(1+\cos^2\psi) + (\varepsilon_1^2 - g^2)\sin^2\psi;$$

$$d = \varepsilon_1(\varepsilon_1^2 - g^2);\ \ \ n^2 = 1 - \frac{2(a-b+d)}{2a - b \pm (b^2 - 4ad)^{1/2}};$$

"+" - "ordinary"; "–" - "extraordinary";

Scattering of HF (MHz) on the regions with increased and decreased electron concentration

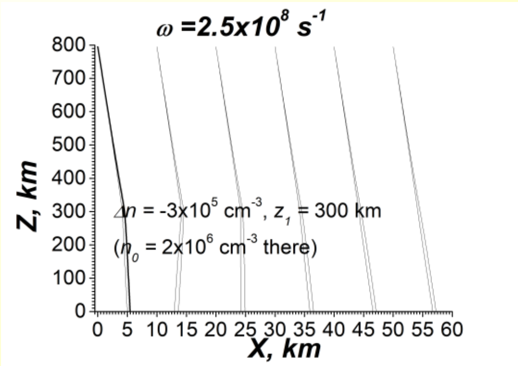

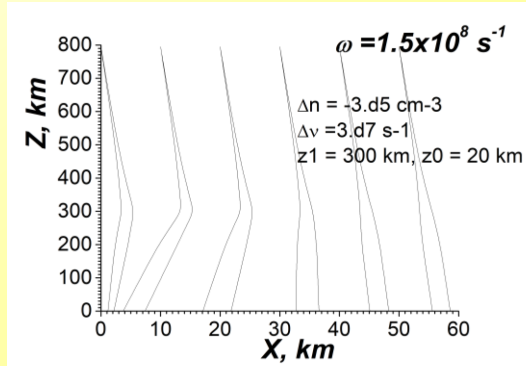

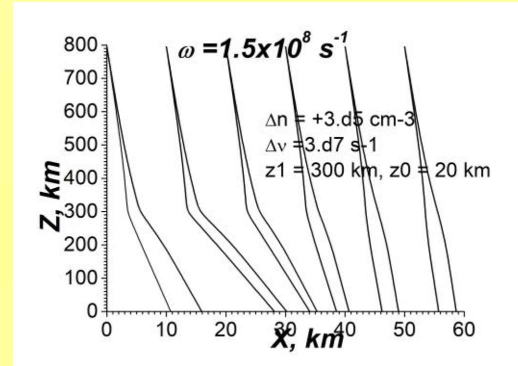

$n=n_0+\Delta n$; $\Delta n<0$

$n=n_0+\Delta n$; $\Delta n>0$

Complex and real geometrical optics

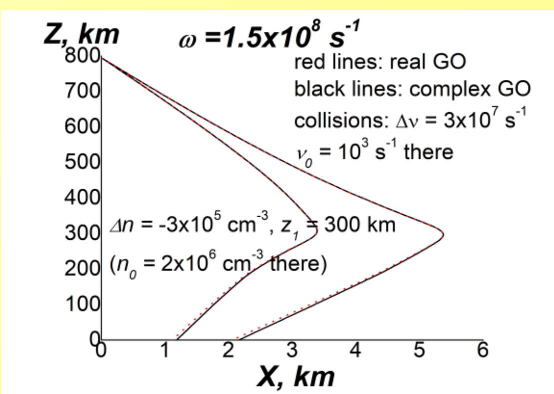

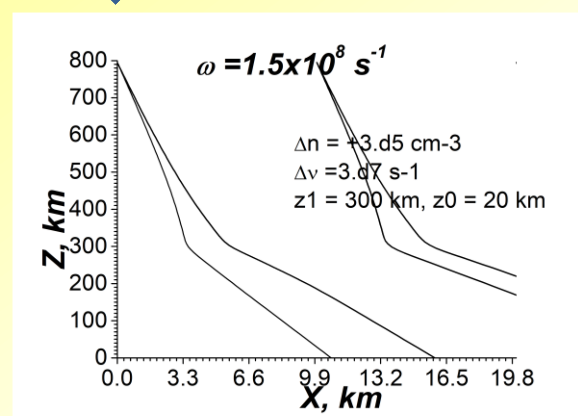

$$n^2 = 1 - \frac{2(a-b+d)}{2a-b\pm(b^2-4ad)^{1/2}};$$ "+" - "ordinary"; "–" - "extraordinary";

Complex geometrical optics: adding dispersion and diffraction and importance of birefringence

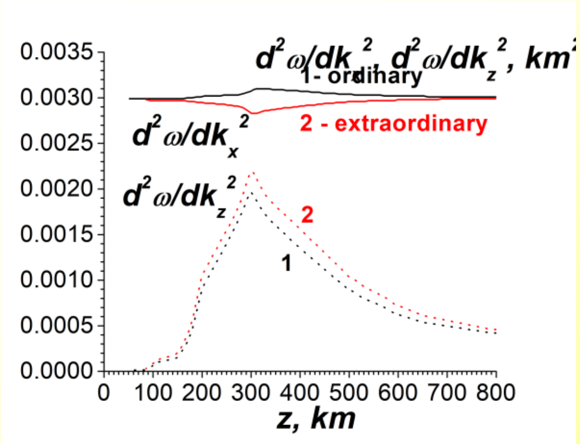

Dispersion diffraction

$\omega=1\cdot10^8 s^{-1}$;
$\Delta n_0=2\cdot10^5\ cm^{-3}$

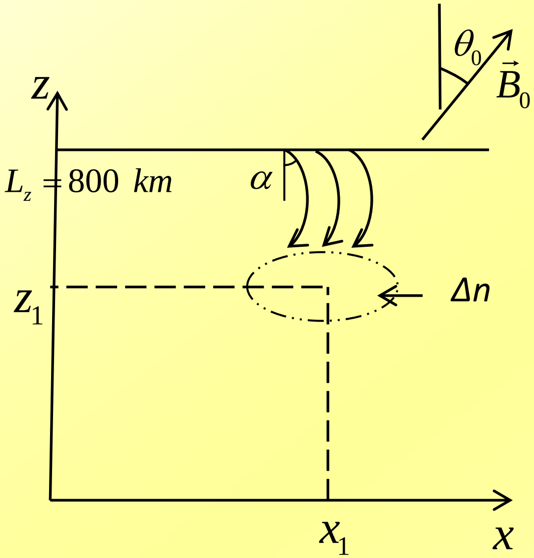

$$\Delta n = \Delta n_0 \exp[-\left(\frac{z-z_1}{z_0}\right)^2 - \left(\frac{x-x_1}{x_0}\right)^2 - \left(\frac{y-y_1}{y_0}\right)^2]$$

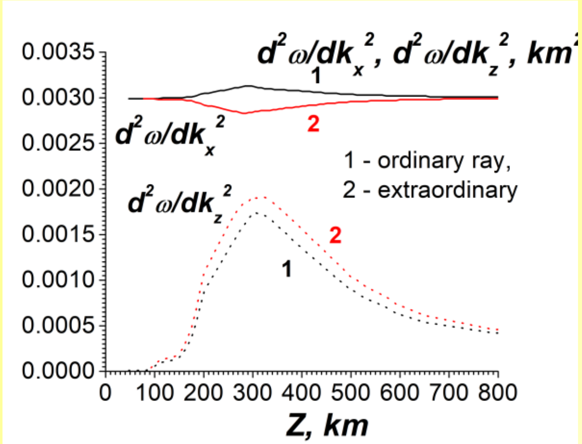

Dispersion diffraction

$\omega=1\cdot10^8 s^{-1}$;
$\Delta n_0=-2\cdot10^5\ cm^{-3}$

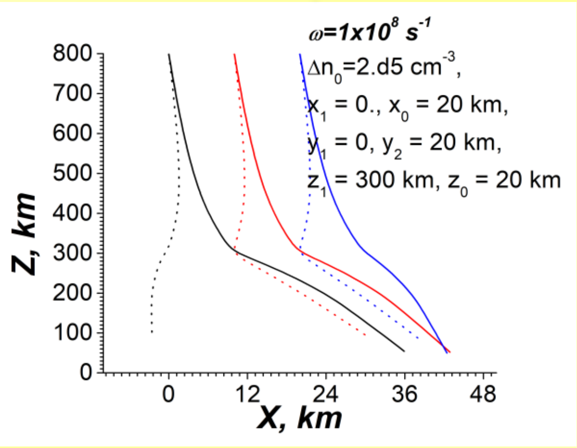

CGO : Scattering of three rays on inhomogeneities with increase and decrease of electron concentration in F region of the ionosphere

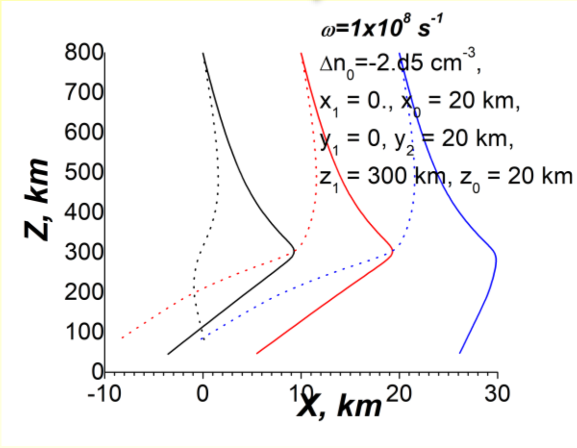

Complex geometrical optics: dispersion, diffraction birefringence and change of frequency due to non-stationarity of ionosphere

$\alpha = \beta = 0.5^\circ;\ \omega = 10^8\ s^{-1};\ \Delta n_0 = 2{,}5\cdot 10^5\ cm^{-3}$

Motion of plasma: $\vec{V} = (V_x, 0\ , 0\ );\ V_x = 1\ km/s$

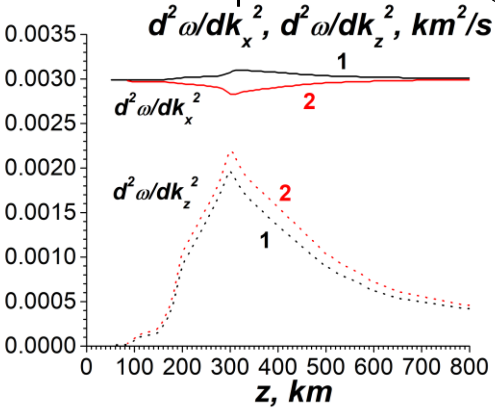

Dispersion and diffraction

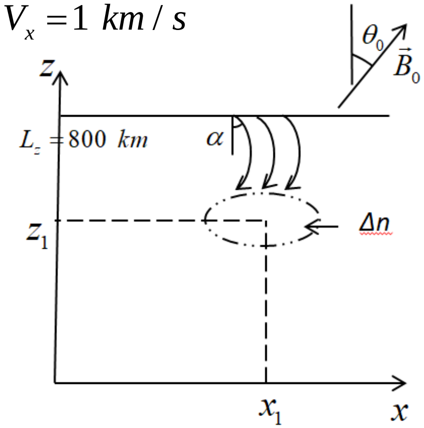

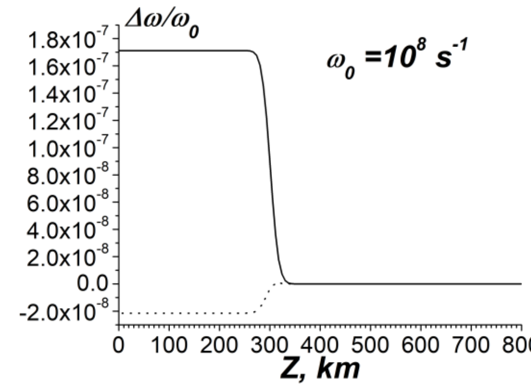

Change in frequency with time due to non-stationarity / motion of plasma

$In\ km: x_1 = 0,\ \ x_0 = 20,\ \ y_1 = 0,\ \ y_0 = 20,\ \ z_1 = 300,\ \ z_0 = 20;$

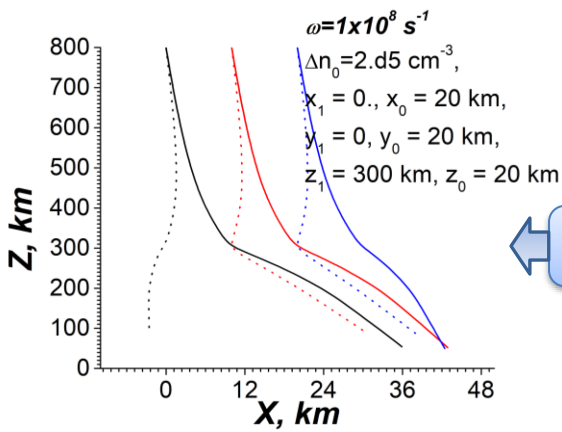

Stationar

Ray tracing: scattering of 3-raybeam / ray on plasma inhomogeneity

Non-stationar

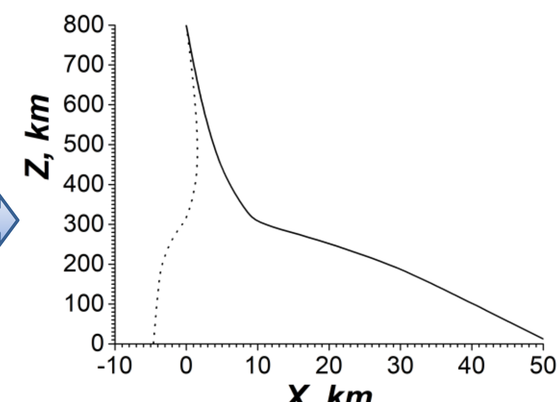

Complex geometrical optics: dispersion, diffraction birefringence and change of frequency due to non-stationarity of ionosphere

$\alpha = \beta = 0.5^\circ;\ \omega = 10^8\ s^{-1};\ \Delta n_0 = -2{,}5 \cdot 10^5\ cm^{-3}$

Motion of plasma: $\vec{V} = (V_x, 0\ , 0\ );\ V_x = 1\ km/s$

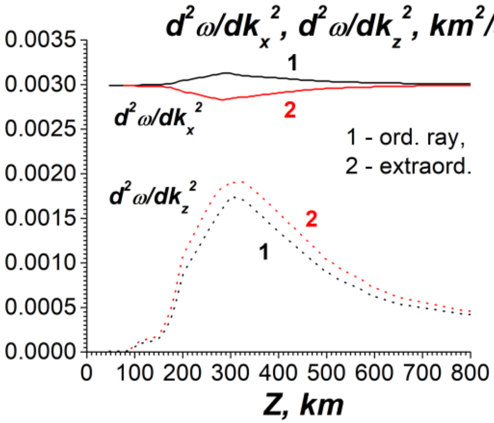

Dispersion and diffraction

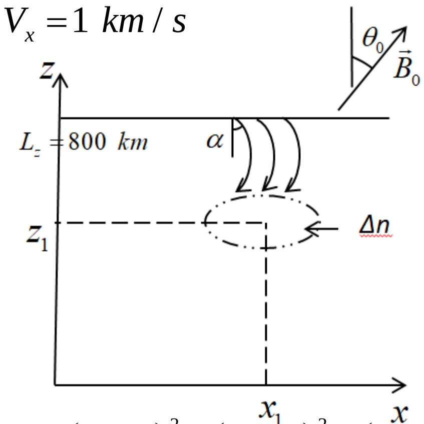

$$\Delta n = \Delta n_0 \exp[-\left(\frac{z - z_1}{z_0}\right)^2 - \left(\frac{x - x_1}{x_0}\right)^2 - \left(\frac{y - y_1}{y_0}\right)^2]$$

$In\ km: x_1 = 0,\ \ x_0 = 20,\ \ y_1 = 0,\ \ y_0 = 20,\ \ z_1 = 300,\ \ z_0 = 20;$

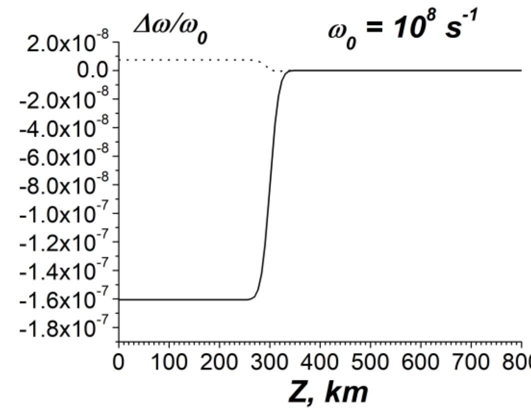

Change in frequency with time due to non-stationarity / motion of plasma

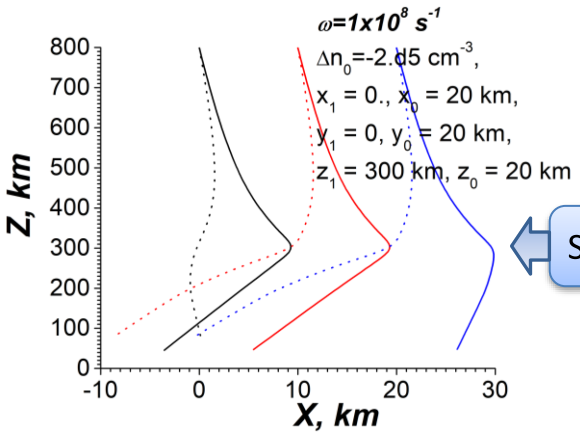

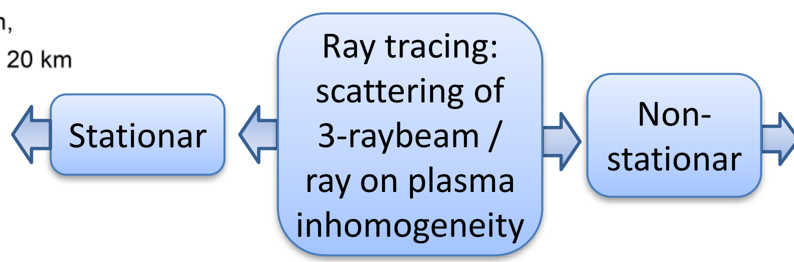

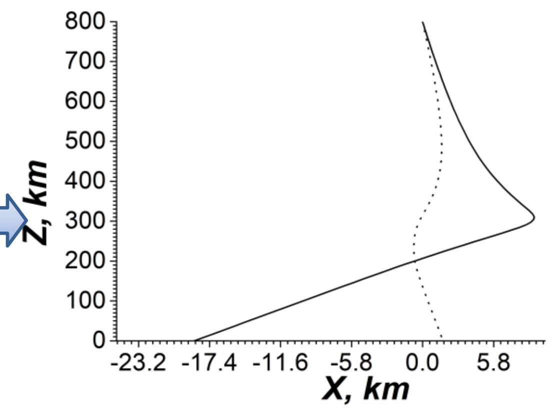

Complex geometrical optics: dispersion, diffraction birefringence and change of frequency due to non-stationarity of ionosphere

$\alpha = 30^{\circ};\ \beta = 0.5^{\circ};\ \omega = 10^{8}\ s^{-1};\ \Delta n_0 = 2{,}5 \cdot 10^{5}\ cm^{-3}$

Motion of plasma: $\vec{V} = (V_x, 0\ , 0\ );\ V_x = 1\ km/s$

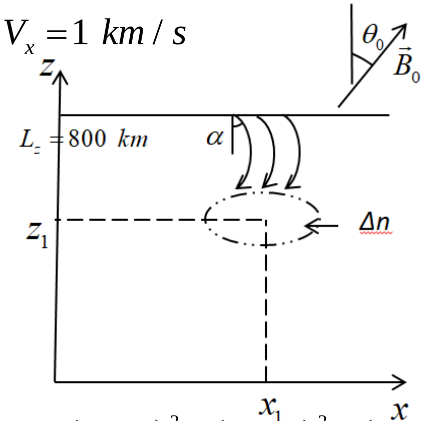

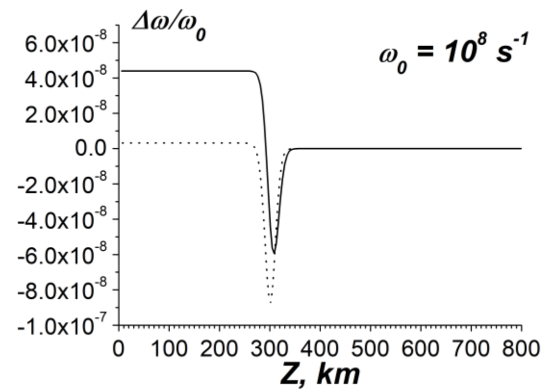

$$\Delta n = \Delta n_0 \exp[-\left(\frac{z - z_1}{z_0}\right)^2 - \left(\frac{x - x_1}{x_0}\right)^2 - \left(\frac{y - y_1}{y_0}\right)^2]$$

$In\ km: x_1 = 0,\ \ x_0 = 20,\ \ y_1 = 0,\ \ y_0 = 20,\ \ z_1 = 300,\ \ z_0 = 20;$

Change in frequency with time due to non-stationarity / motion of plasma

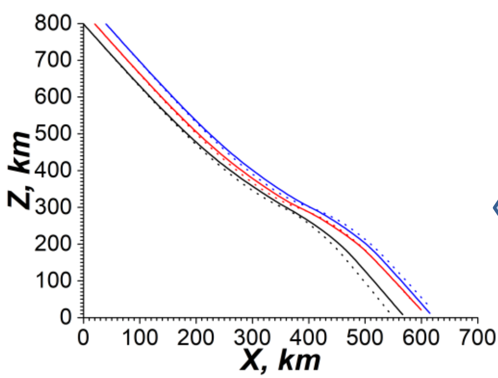

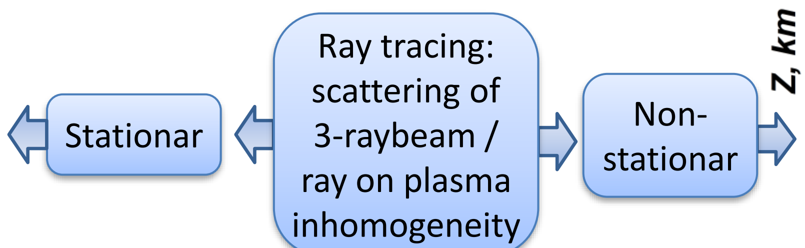

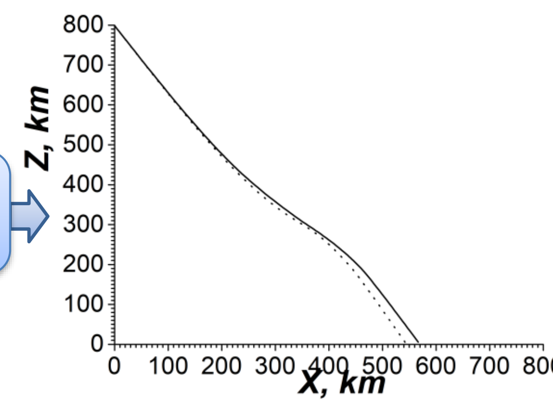

Complex geometrical optics: dispersion, diffraction birefringence and change of frequency due to non-stationarity of ionosphere

$\alpha = 30^{\circ}; \ \beta = 0.5^{\circ}; \ \omega = 10^{8} \ s^{-1}; \ \Delta n_0 = -2{,}5 \cdot 10^{5} \ cm^{-3}$

Motion of plasma: $\vec{V} = (V_x, 0\ , 0\ ); \ V_x = 1 \ km/s$

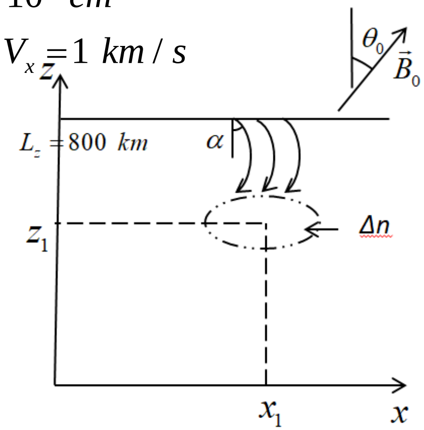

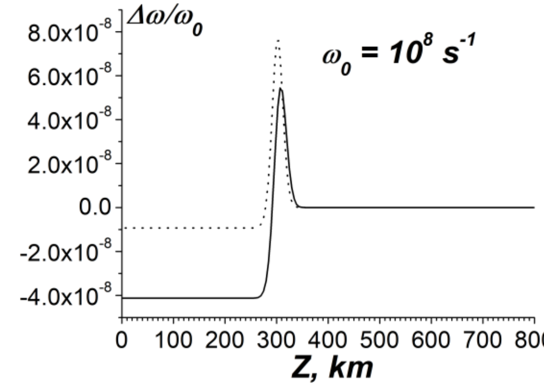

$In \ km: x_1 = 0, \ x_0 = 20, \ y_1 = 0, \ y_0 = 20, \ z_1 = 300, \ z_0 = 20;$

Change in frequency with time due to non-stationarity / motion of plasma

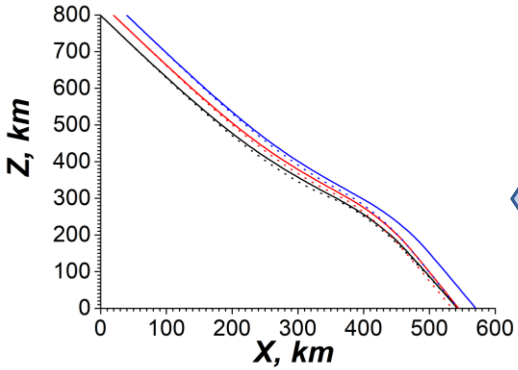

Stationar

Ray tracing: scattering of 3-raybeam / ray on plasma inhomogeneity

Non-stationar

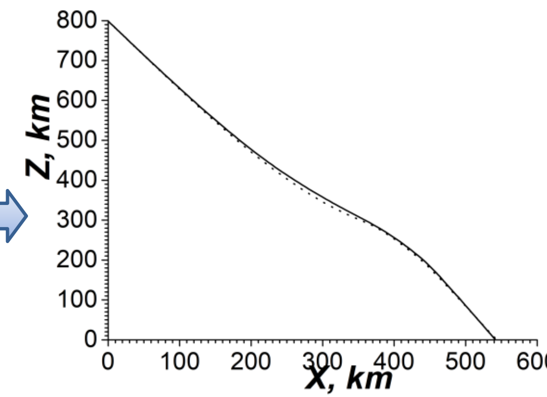

Complex geometrical optics: dispersion, diffraction birefringence and change of frequency due to non-stationarity of ionosphere

$\alpha = 15^{\circ};\ \beta = 0^{\circ};\ \omega = 10^{8}\ s^{-1};\ \Delta n_0 = -2{,}5\cdot 10^{5}\ cm^{-3}$

Motion of plasma: $\vec{V} = (V_x, 0\ ,0\ );\ V_x = 1\ km/s$

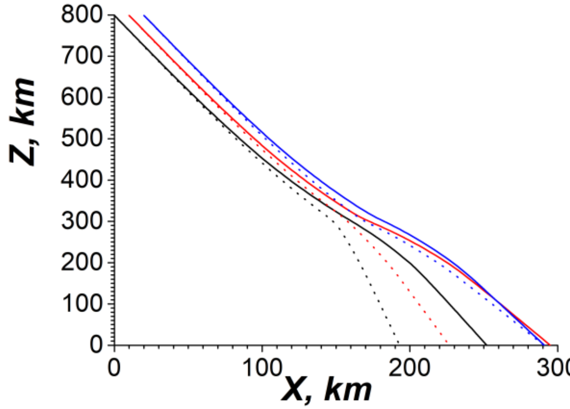

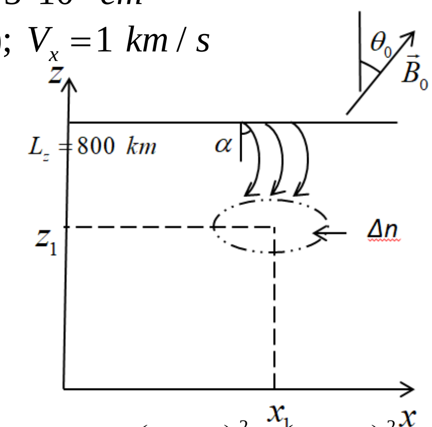

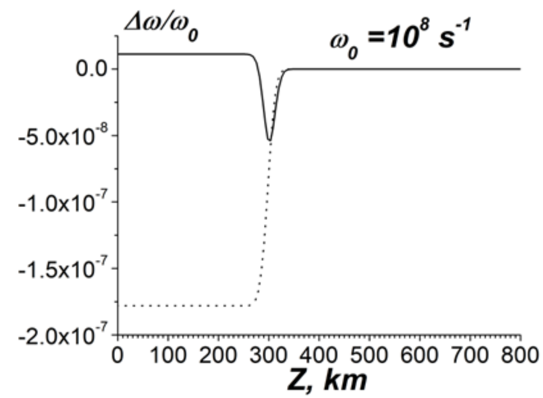

$$\Delta n = \Delta n_0 \exp[-\left(\frac{z-z_1}{z_0}\right)^2 - \left(\frac{x-x_1}{x_0}\right)^2 - \left(\frac{y-y_1}{y_0}\right)\ ]$$

$In\ km: x_1 = 0,\ \ x_0 = 20,\ \ y_1 = 0,\ \ y_0 = 20,\ \ z_1 = 300,\ \ z_0 = 20;$

Tray

$+2{,}5\cdot 10^{5}\ cm^{-3}$

$-2{,}5\cdot 10^{5}\ cm^{-3}$

Δn_0

$+2{,}5\cdot 10^{5}\ cm^{-3}$

$-2{,}5\cdot 10^{5}\ cm^{-3}$

$\Delta\omega(t;z)$

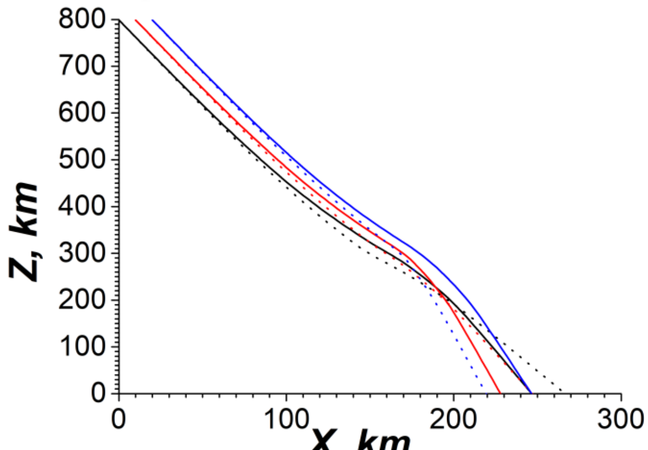

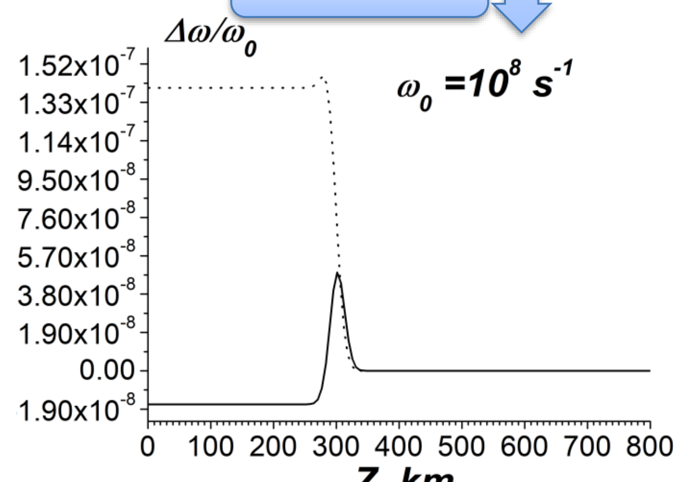

Conclusions and future work

1) Complex geometrical optics (CGO) for comparison of LOFAR-GNSS observations with theory of EMW propagation and scattering on TIDs and other plasma structures in the unstable ionosphere; accounting for birefringence, dispersion, diffraction, change of wave frequency due to non-stationarity of the ionosphere;

1) TIDs : L_{opt}=KL >>1 ⇨ opposite to thin ionosphere/thin screen approximation;

2) Instability *F*-E_S : Developing Ionosphere Plasma Structure may cover all the (*E*-*F*) altitude range of ionosphere, where TEC is formed;

3) Scattering of Radio Waves (RWs) of plasma inhomogeneities;

4) CGO: change of **ω** due to non-stationary; **ω= ω(z, t): z → t; ω= ω(t)**; **Δn** of opposite sign → extreme of different signs of **Δω(z).**

For the future work:

- Modelling TIDs accounting for: (1)their propagation is non-horizontal; (2) presence of wind; (3) presence of photochemistry processes; (4) forming TIDs under influence of AGWs;
- 3D Modeling formation and propagation of Ionospheric Plasma Structures (IPS) accounting for (a) instability such as Es, Perking and combined Es-Perking instabilities in all the range of altitudes of E and F regions of Ionosphere, where TEC is formed; (b) plasma nonlinearity;
- Modeling scattering RWs on IPS/TIDs for the conditions of different levels of solar/geophysical activity; including period of solar maximum 2023-2025, with increased Ne/TEC, strong-gradient IPS/TIDs formation in all the ionosphere; and expected penetration of the IPS/TIDs with extreme parameters (amplitudes, gradients) from high- and low- to middle-latitude region; accounting for scintillations in the ionosphere.
- Modeling-base determination of the conditions of applicability/no-applicability of the approximations of “optically thin ionosphere/scattering screens”, ergodicity etc.

Dear colleagues!

We cordially invite you to present your research in a special issue of the MDPI Remote Sensing journal with IF=5.349:

https://www.mdpi.com/journal/remotesensing/special_issues/O7I27D1I49

"Satellite and Ground-Based Remote Sensing of Seismic, Volcanic and Cyclonic Activity in the Earth-Atmosphere-Ionosphere System". Prof. Dr. Yuriy G. Rapoport (Yuriy.Rapoport@gmail.com), Prof. Dr. Volodymyr Grimalsky (v_grim@hotmail.com), Dr. Anatoly Kotsarenko (akotsarenko@pampano.unacar.mx) and Dr. Gianfranco Cianchini (gianfranco.cianchini@ingv.it) are serving as Guest Editors for this Special Issue. The deadline indicated on the site now is 06/30/2023, but in fact, articles can be sent, in agreement with the Editorial Board (Ms. Suzy Guo, Section Managing Editor, MDPI Nanjing) until 09/30/2023. If you intend to submit your article to this special issue and would like to receive an invitation from Guest Editors with a 50% discount on the payment for this publication, please send an email indicating the tentative topic of the paper to the invited editors.

Conclusions concerning ULF anf VLF processes in the Earth-Atmosphere-Ionosphere system including waveguide Earth-Ionosphere (WGEI)

I.The methods for modelling ULF electromagnetic and AGW channels of coupling in the system “Earth–atmosphere–ionosphere” and VLF propagation in WGEI has been developed.

II.Signal is processed with Fourier, wavelet and information entropy approaches. Oscillations of 5–10 min, 20–40 min, 3 hour, 7 days are revealed in VLF/WGEI data.

III.In the theory of atmospheric electricity (TAE) – magnetic is lost! → modification of TAE / global eclectic circuit (GEC) models – is modified!

IV.Powerful Volcano Eruption (f.e. Hunga-Tonga) can excitation the coupled Schumann-Alfven resonator. Such excitation is a remarkable manifestation of an influence on Space Weather „From the sources placed below the ionosphere”; boundary conditions used for the modelling: at the Earth and at Z=800 km. Excitation of Alfven resonator by local powerful source has the global character and can pronounced itself brightly, in particular of Hunga-Tonga Volcano eruption-excitation event, f.e. at Finland coordinates.